J|A|C|S ARTICLES

Published on Web 04/14/2009

# Single-Conformation and Diastereomer Specific Ultraviolet and Infrared Spectroscopy of Model Synthetic Foldamers: α/β-Peptides

William H. James III,[†] Esteban E. Baquero,[†,‡] V. Alvin Shubert,[†,§] Soo Hyuk Choi,[⊥,¶] Samuel H. Gellman,[⊥] and Timothy S. Zwier*,[†]

*Department of Chemistry, Purdue University, 560 Oval Drive, West Lafayette, Indiana 47907-2084, and Department of Chemistry, University of Wisconsin, Madison, Wisconsin 53706*

Received February 10, 2009; E-mail: zwier@purdue.edu

***Abstract:*** Resonant two-photon ionization (R2PI), UV hole-burning (UVHB), and resonant ion-dip infrared (RIDIR) spectroscopies have been used to record single-conformation infrared and ultraviolet spectra of three model synthetic foldamers with heterogeneous backbones, α/β-peptides Ac-$\beta^3$-hAla-L-Phe-NHMe (**βαL**), Ac-$\beta^3$-hAla-D-Phe-NHMe (**βαD**), and Ac-L-Phe-$\beta^3$-hAla-NHMe (**αβL**), isolated and cooled in a supersonic expansion. **βαL** and **βαD** are diastereomers, differing only in the configuration of the α-amino acid residue; **βαL** and **αβL** contain the same residues, but differ in residue order. In all three α/β-peptides the $\beta^3$-residue has *S* absolute configuration. UVHB spectroscopy is used to determine that there are six conformers of each molecule and to locate and characterize their $S_0-S_1$ transitions in the origin region. RIDIR spectra in the amide NH stretch region reflect the number and strength of intramolecular H-bonds present. Comparison of the RIDIR spectra with scaled, harmonic vibrational frequencies and infrared intensities leads to definite assignments for the conformational families involved. C8/$C7_{eq}$ double-ring structures are responsible for three conformers of **βαL** and four of **βαD**, including those with the most intense transitions in the R2PI spectra. This preference for C8/$C7_{eq}$ double rings appears to be dictated by the $C7_{eq}$ ring of the α-peptide subunit. Three of the conformers of **βαL** and **βαD** form diastereomeric pairs (A/A′, C/C′, and G/G′) that have nearly identical $S_0-S_1$ origin positions in the UV and belong to the same conformational family, indicating no significant change associated with the change in chirality of the α-peptide subunit. However, **βαL** favors formation of a C6/C5 conformer over C11, while the reverse preference holds in **βαD**. Calculations indicate that the selective stabilization of the lowest-energy C11($g_+$) structure in **βαD** occurs because this structure minimizes steric effects between the $\beta^2$ methylene group and C=O(1). In the α/β-peptide **αβL**, two conformers dominate the spectrum, one assigned to a C5/C8 bifurcated double-ring, and the other to a C5/C6 double-ring structure. This preference for C5 rings in the α/β-peptide occurs because the C5 ring is further stabilized by an amide NH$\cdots\pi$ interaction involving an NH group on the adjacent amide, as it is in the α-peptides. Comparison of the NH stretch spectra of C8/$C7_{eq}$ structures in **βαL** with their $C7_{eq}$/C8 counterparts in **αβL** shows that the central amide NH stretch is shifted to lower frequency by some 50−70 $cm^{-1}$ due to cooperative effects associated with the central amide accepting and donating a H-bond to neighboring amide groups. This swaps the ordering of the C8 and C7 NH stretch fundamentals in the two molecules.

## 1. Introduction

In naturally occurring peptides and proteins, 20 α-amino acids serve as building blocks to produce oligo- or polypeptides in which the backbone amide groups are separated by a single substituted carbon atom. The synthesis of oligomers containing alternative, custom-designed monomer units can lead to new folding propensities.[1−7] Among the various classes of synthetic foldamers, β-peptides, which differ from α-peptides in having a second carbon atom separating the amide groups, have played an especially important role.[1,2,6,7] By varying the position and nature of the substituents on the $\beta^2$ and/or $\beta^3$ carbons, the propensity for forming helices with a well-defined pitch can be controlled. As in α-peptides, most secondary structures of β-peptides are associated with specific patterns of interamide H-bonds (NH$\cdots$O=C).

[†] Purdue University.
[‡] Present address: Process Analytical, The Dow Chemical Company, 2301 N. Brazosport Blvd. B-1463, Freeport, TX 77541.
[§] Present address: Argonne National Laboratory, Chemistry Division, Argonne, IL 60439.
[⊥] University of Wisconsin.
[¶] Present address: Department of Chemistry, Northwestern University, Evanston, IL 60208-3113.

(1) Cheng, R. P.; Gellman, S. H.; DeGrado, W. F. *Chem. Rev.* **2001**, *101*, 3219.
(2) Gellman, S. H. *Acc. Chem. Res.* **1998**, *31*, 173.
(3) Hecht, S.; Huc, I. *Foldamers: Structure, Properties, and Applications*; Wiley-VCH: Weinheim, 2007.
(4) Hill, D. J.; Mio, M. J.; Prince, R. B.; Hughes, T. S.; Moore, J. S. *Chem. Rev.* **2001**, *101*, 3893.
(5) Huc, I. *Eur. J. Org. Chem.* **2004**, 17.
(6) Seebach, D.; Cardiner, J. *Acc. Chem. Res.* **2008**, *41*, 1366.
(7) Seebach, D.; Matthews, J. L. *Chem. Commun.* **1997**, 2015.


**10.1021/ja901051v CCC: $40.75** 

We have recently studied the inherent conformational preferences and spectral signatures of a set of four model $\beta$-peptides using laser spectroscopy of the isolated molecules cooled in a supersonic expansion.[8,9] By incorporating a phenylalanine side chain into the $\beta$-peptide backbone, we were able to use resonant two-photon ionization to record ultraviolet spectra. Then, using double-resonance depletion spectroscopy, we recorded the single-conformation infrared and ultraviolet spectra, providing the inherent spectral signatures of model secondary structural elements. In the smallest of these molecules, Ac-$\beta^3$-hPhe-NHMe, both 6-membered (C6) and 8-membered (C8) H-bonded rings were formed, with the C6 conformer dominating the spectrum. The larger molecules Ac-$\beta^3$-hPhe-$\beta^3$-hAla-NHMe and Ac-$\beta^3$-hAla-$\beta^3$-hPhe-NHMe showed a rich conformational makeup, with C6/C6 and C8/C8 double rings, C10 single rings, and C6/C8 double ring-double acceptor structures present.

This study complemented earlier work of a similar nature on short α-peptides.[10−14] In the case of α-peptides, H-bonds linking adjacent amide groups (a→a ± 1) lead to either C5 or C7 H-bonded rings, while larger C10 rings were formed between next nearest-neighbor amide groups. The longer α-peptides also showed double-ring structures composed of C5/C7, C7/C7, C7/C10, or C10/C10 double rings.

Recently, synthetic foldamers containing both α- and $\beta$-amino acid residues ("α/$\beta$-peptides") have gained increasing attention.[15−23] These mixed subunit oligomers add further diversity to the structural pool via control of the position and pattern of α- and $\beta$-subunits. Mixing subunit classes changes the type of H-bonded rings that can be formed, opening up a wider variety of structural motifs. Well-defined helical secondary structures have been documented among α/$\beta$-peptides with a variety of intramolecular H-bond patterns, and small hairpin folding patterns have been observed as well.[20] The conformational preferences underlie recent biological applications of α/$\beta$-peptides, including as antibacterial agents[16,17] and as antagonists of protein−protein interactions[19,24] As with the $\beta$-peptides themselves,[8,9] far less is known about the conformational preferences and spectral signatures of α/$\beta$-peptides than about α-peptides, which creates an opportunity to use the tools of laser spectroscopy for elucidation of folding behavior. We report here the single-conformation infrared and ultraviolet spectra of isomeric α/$\beta$-peptides Ac-$\beta^3$-hAla-L-Phe-NHMe (**βαL**), Ac-$\beta^3$-hAla-D-Phe-NHMe (**βαD**) and Ac-L-Phe-$\beta^3$- hAla-NHMe (**αβL**), isolated and cooled in a supersonic expansion.

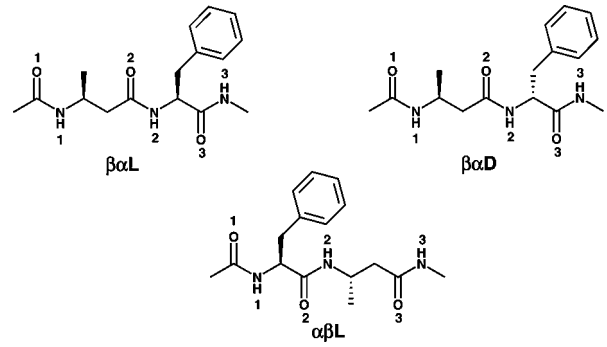


As with previous studies,[8−12,14,25−33] the incorporation of the phenylalanine side chain makes it possible to use double resonance schemes to record the single-conformation spectra free from interference from one another, thereby providing their fundamental spectral signatures free from influence of solvent, for direct comparison with the predictions of computational chemistry.

α/$\beta$-Peptides **βαL**, **βαD**, and **αβL** each have two stereogenic centers, one on the α-carbon of the α-residue and the other at the $\beta^3$ position of the $\beta$-residue. **βαL** and **αβL** are sequence-isomers, since they contain the same residues, but in differing order. **βαL** and **βαD** are diastereomers, since they differ only in the configuration of the stereogenic center in the phenylalanine residue. Naturally occurring proteins are made up of α-amino acids with exclusively L configuration, but some natural peptides derived from nonribosomal biosynthesis contain residues with both L and D configuration, and combining configurations has been shown to be extremely fruitful with respect to peptide and protein design.[34] Therefore, it is of fundamental interest to explore the impact of changing a single stereogenic

(8) Baquero, E. E.; James, W. H.; Choi, S. H.; Gellman, S. H.; Zwier, T. S. *J. Am. Chem. Soc.* **2008**, *130*, 4784.
(9) Baquero, E. E.; James, W. H.; Choi, S. H.; Gellman, S. H.; Zwier, T. S. *J. Am. Chem. Soc.* **2008**, *130*, 4795.
(10) Chin, W.; Piuzzi, F.; Dognon, J. P.; Dimicoli, I.; Mons, M. *J. Chem. Phys.* **2005**, *123*, 084301.
(11) Chin, W.; Piuzzi, F.; Dimicoli, I.; Mons, M. *Phys. Chem. Chem. Phys.* **2006**, *8*, 1033.
(12) Chin, W.; Dognon, J. P.; Canuel, C.; Piuzzi, F.; Dimicoli, I.; Mons, M.; Compagnon, I.; von Helden, G.; Meijer, G. *J. Chem. Phys.* **2005**, *122*, 054317.
(13) Gerhards, M.; Unterberg, C.; Gerlach, A.; Jansen, A. *Phys. Chem. Chem. Phys.* **2004**, *6*, 2682.
(14) Chin, W.; Mons, M.; Dognon, J. P.; Mirasol, R.; Chass, G.; Dimicoli, I.; Piuzzi, F.; Butz, P.; Tardivel, B.; Compagnon, I.; von Helden, G.; Meijer, G. *J. Phys. Chem. A* **2005**, *109*, 5281.
(15) Choi, S. H.; Guzei, I. A.; Spencer, L. C.; Gellman, S. H. *J. Am. Chem. Soc.* **2008**, *130*, 6544.
(16) Schmitt, M. A.; Weisblum, B.; Gellman, S. H. *J. Am. Chem. Soc.* **2004**, *126*, 6848.
(17) Schmitt, M. A.; Weisblum, B.; Gellman, S. H. *J. Am. Chem. Soc.* **2007**, *129*, 417.
(18) Hayen, A.; Schmitt, M. A.; Ngassa, F. N.; Thomasson, K. A.; Gellman, S. H. *Angew. Chem., Int. Ed.* **2004**, *43*, 505.
(19) Horne, W. S.; Boersma, M. D.; Windsor, M. A.; Gellman, S. H. *Angew. Chem., Int. Ed.* **2008**, *47*, 2853.
(20) Horne, W. S.; Gellman, S. H. *Acc. Chem. Res.* **2008**, *41*, 1399.
(21) Horne, W. S.; Price, J. L.; Keck, J. L.; Gellman, S. H. *J. Am. Chem. Soc.* **2007**, *129*, 4178.
(22) Price, J. L.; Horne, W. S.; Gellman, S. H. *J. Am. Chem. Soc.* **2007**, *129*, 6376.
(23) Schmitt, M. A.; Choi, S. H.; Guzei, I. A.; Gellman, S. H. *J. Am. Chem. Soc.* **2006**, *128*, 4538.
(24) Sadowsky, J. D.; Fairlie, W. D.; Hadley, E. B.; Lee, H. S.; Umezawa, N.; Nikolovska-Coleska, Z.; Wang, S. M.; Huang, D. C. S.; Tomita, Y.; Gellman, S. H. *J. Am. Chem. Soc.* **2007**, *129*, 139.
(25) Gloaguen, E.; Pagliarulo, F.; Brenner, V.; Chin, W.; Piuzzi, F.; Tardivel, B.; Mons, M. *Phys. Chem. Chem. Phys.* **2007**, *9*, 4491.
(26) Brenner, V.; Piuzzi, F.; Dimicoli, I.; Tardivel, B.; Mons, M. *J. Phys. Chem. A* **2007**, *111*, 7347.
(27) Brenner, V.; Piuzzi, F.; Dimicoli, I.; Tardivel, B.; Mons, M. *Angew. Chem., Int. Ed.* **2007**, *46*, 2463.
(28) Chin, W.; Piuzzi, F.; Dognon, J. P.; Dimicoli, L.; Tardivel, B.; Mons, M. *J. Am. Chem. Soc.* **2005**, *127*, 11900.
(29) Chin, W.; Dognon, J. P.; Piuzzi, F.; Dimicoli, I.; Mons, M. *Mol. Phys.* **2005**, *103*, 1579.
(30) Chass, G. A.; Mirasol, R. S.; Setiadi, D. H.; Tang, T. H.; Chin, W.; Mons, M.; Dimicoli, I.; Dognon, J. P.; Viskolcz, B.; Lovas, S.; Penke, B.; Csizmadia, I. G. *J. Phys. Chem. A* **2005**, *109*, 5289.
(31) Chin, W.; Compagnon, I.; Dognon, J. P.; Canuel, C.; Piuzzi, F.; Dimicoli, I.; von Helden, G.; Meijer, G.; Mons, M. *J. Am. Chem. Soc.* **2005**, *127*, 1388.
(32) Chin, W.; Dognon, J. P.; Piuzzi, F.; Tardivel, B.; Dimicoli, I.; Mons, M. *J. Am. Chem. Soc.* **2005**, *127*, 707.
(33) Chin, W.; Mons, M.; Dognon, J. P.; Piuzzi, F.; Tardivel, B.; Dimicoli, I. *Phys. Chem. Chem. Phys.* **2004**, *6*, 2700.
(34) Durani, S. *Acc. Chem. Res.* **2008**, *41*, 1301.

center on the conformational propensities of our short α/β-peptides. As we shall see, the effect of this subtle change is significant.

There are other recent examples in which jet-cooled laser spectroscopy has been used to study diastereomer-specific conformational behavior, most notably in work on α-peptides by the groups of Mons[25,27] and de Vries,[35] and the study of ephedrine/pseudoephedrine by Simons and co-workers.[36] In addition, Zehnacker-Rentien and co-workers have carried out analogous studies on complexes formed from two chiral molecules, which probe both inter- and intramolecular interactions.[37−39] The results presented here represent a distinctive addition to a growing body of work in which the combination of jet-cooling with double-resonance spectroscopy provides the unique spectral signatures of individual conformations for a pair of diastereomers. As we shall see, such studies can provide unique insights into the influence of chirality on the intramolecular interactions experienced by each molecule, leading to diastereomer-specific conformational propensities.

## 2. Experimental and Computational Methods

**2.1. Experimental Methods.** The syntheses of **βαL**, **βαD**, and **βαL** were carried out using standard methods as described in the Supporting Information. The experimental methods used to record single-conformation infrared and ultraviolet spectra have been described in detail elsewhere.[8,9,40] Here we summarize those aspects of direct relevance to the present work. The solid peptide samples were introduced into the gas phase by heating the sample contained in a stainless steel sample holder fixed directly before the pulsed valve. Operating temperatures of approximately 215−225 °C were needed to obtain sufficient vapor pressure for these studies. In order to minimize thermal decomposition, the solid sample was held in a glass insert inside the sample holder in order to minimize contact with the metal walls of the sample holder. A pulsed valve with 400 μm orifice diameter (Parker General Valve, series 9) was used in forming the supersonic expansion. The samples were entrained in a 70%/30% neon/helium mixture with a backing pressure of 1.5 bar and expanded into vacuum, with typical flow rates of 0.15−0.30 bar·cm$^3$/s.

Resonant two-photon ionization (R2PI) spectroscopy was utilized to record the ultraviolet spectra of the molecules in the $S_0-S_1$ region of the phenylalanine side chain. The samples were excited with the frequency doubled output of a Nd:YAG pumped tunable dye laser. Typical ultraviolet laser powers used were 0.1−0.5 mJ/pulse. The ultraviolet light traversed the ionization region of the TOF as a collimated beam (∼1 mm diam.) The resultant ions were detected by a micro channel plate detector atop a 1-m-long flight tube.

Conformation specific electronic spectra were obtained using ultraviolet hole-burning spectroscopy (UVHB). UVHB spectra were recorded using a high power hole-burning laser (0.5−0.75 mJ/pulse, 10 Hz) fixed on a transition in the R2PI spectrum, while a probe laser (0.1−0.5 mJ/pulse, 20 Hz) was tuned through the region of interest in the R2PI spectrum. The hole-burn and probe lasers were counter-propagated, spatially overlapped, and temporally separated by 200 ns, with the hole-burn laser preceding the probe. The integrated ion signal was probed using active baseline subtraction in a gated integrator to observe the difference in ion signal due to the probe laser with the hole-burn laser 'on' vs 'off'. Probe laser transitions arising from the same ground-state level as the hole-burn transition resulted in depletions in ion signal.

Conformation-specific infrared spectra were recorded using resonant ion-dip infrared spectroscopy (RIDIRS).[41,42] Tunable infrared radiation was obtained using a seeded Nd:YAG pumped parametric converter (LaserVision). Infrared laser energies of 1−5 mJ/pulse were typically used. In a manner similar to UVHB, the IR (10 Hz) and UV (20 Hz) were counter-propagated, spatially overlapped, and temporally separated by 200 ns, with the IR pulse preceding the UV probe pulse. The UV probe was fixed on a transition of interest in the R2PI spectrum due to a single conformational isomer, while the IR was tuned over the spectral range 3200−3500 cm$^{-1}$. The ion signal resulting from the UV probe was monitored while the IR was tuned. IR transitions resulting from the same ground-state level as the probed transition produced depletions in the ion signal due to the conformational isomer of interest. A gated integrator operating in active baseline subtraction mode was utilized to record the conformation-specific IR spectra.

**2.2. Computational Methods.** In order to identify low-lying conformational minima of **βα** and **αβ**, we carried out an initial screening for possible conformational minima using the Amber force field[43] within the MACROMODEL suite of programs.[44] The random search of conformational space resulted in approximately 190 starting structures within a 70 kJ/mol energy window for each of the molecules. The starting structures obtained from the MACROMODEL search were then used as input structures for investigation with density functional theory using B3LYP functional[45,46] and 6-31+G(d) basis set,[47] within the GAUSSIAN 03 suite of programs.[48]

Since standard DFT B3LYP calculations do not properly account for dispersion,[49−53] relative energies were computed using two alternative methods. Single-point second-order Møller−Plesset perturbation theory (MP2)[54] calculations employing the same 6-31+G(d) basis set explicitly account for electron correlation effects. However, they also suffer from large intramolecular basis set superposition error in calculations that employ all but the very largest basis sets, as has recently been explored in some detail by van Mourik and co-workers.[52,53] They also give a systematic overestimation of dispersion. As a result, we also carried out optimizations on a subset of the DFT B3LYP/6-31+G(d) minima using the recently developed M05-2X functional[49] with a 6-31+G(d) basis set. This functional was designed to better account for dispersive interactions and is finding increasing use in circumstances where dispersion is important.[51,55−60] These calculations were preformed using the computational resources of GridChem.[61,62]


(35) Abo-Riziq, A. G.; Bushnell, J. E.; Crews, B.; Callahan, M. P.; Grace, L.; De Vries, M. S. *Int. J. Quantum Chem.* **2005**, *105*, 437.
(36) Butz, P.; Kroemer, R. T.; Macleod, N. A.; Simons, J. P. *Phys. Chem. Chem. Phys.* **2002**, *4*, 3566.
(37) Le Barbu-Debus, K.; Broquier, M.; Mahjoub, A.; Zehnacker-Rentien, A. *J. Phys. Chem. A* **2008**, *112*, 9731.
(38) Le Barbu-Debus, K.; Lahmani, F.; Zehnacker-Rentien, A.; Guchhait, N.; Panja, S. S.; Chakraborty, T. *J. Chem. Phys.* **2006**, *125*, 174305.
(39) Seurre, N.; Le Barbu-Debus, K.; Lahmani, F.; Zehnacker-Rentien, A. *Actualite Chim.* **2004**, 29.
(40) Shubert, V. A.; Baquero, E. E.; Clarkson, J. R.; James, W. H.; Turk, J. A.; Hare, A. A.; Worrel, K.; Lipton, M. A.; Schofield, D. P.; Jordan, K. D.; Zwier, T. S. *J. Chem. Phys.* **2007**, *127*, 234315.
(41) Zwier, T. S. *Annu. Rev. Phys. Chem.* **1996**, *47*, 205.
(42) Page, R. H.; Shen, Y. R.; Lee, Y. T. *J. Chem. Phys.* **1988**, *88*, 4621.
(43) Weiner, P. K.; Kollman, P. A. *J. Comput. Chem.* **1981**, *2*, 287.
(44) Mohamadi, F.; Richards, N. G. J.; Guida, W. C.; Liskamp, R.; Lipton, M.; Caufield, C.; Chang, G.; Hendrickson, T.; Still, W. C. *J. Comput. Chem.* **1990**, *11*, 440.
(45) Becke, A. D. *J. Chem. Phys.* **1993**, *98*, 5648.
(46) Lee, C. T.; Yang, W. T.; Parr, R. G. *Phys. Rev. B* **1988**, *37*, 785.
(47) Frisch, M. J.; Pople, J. A.; Binkley, J. S. *J. Chem. Phys.* **1984**, *80*, 3265.
(48) Frisch, M. J.; et al. *Gaussian 03*, Revision E.01; Gaussian, Inc.: Wallingford, CT, 2004. The full reference is given in the Supporting Information.
(49) Zhao, Y.; Truhlar, D. G. *J. Chem. Theory Comput.* **2007**, *3*, 289.
(50) Wodrich, M. D.; Corminboeuf, C.; Schleyer, P. V. *Org. Lett.* **2006**, *8*, 3631.
(51) Wodrich, M. D.; Corminboeuf, C.; Schreiner, P. R.; Fokin, A. A.; Schleyer, P. V. *Org. Lett.* **2007**, *9*, 1851.
(52) Holroyd, L. F.; van Mourik, T. *Chem. Phys. Lett.* **2007**, *442*, 42.
(53) Shields, A. E.; van Mourik, T. *J. Phys. Chem. A* **2007**, *111*, 13272.
(54) Moller, C.; Plesset, M. S. *Phys. Rev.* **1934**, *46*, 0618.
(55) Barone, V.; Biczysko, M.; Pavone, M. *Chem. Phys.* **2008**, *346*, 247.
(56) Leverentz, H. R.; Truhlar, D. G. *J. Phys. Chem. A* **2008**, *112*, 6009.

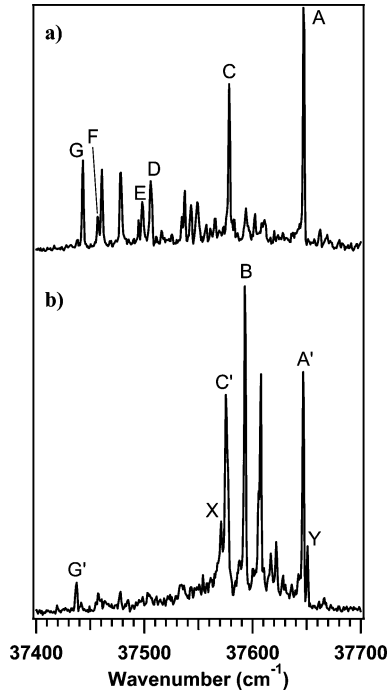


***Figure 1.*** (a) R2PI spectrum of ***β*α**L. (b) R2PI spectrum of ***β*α**D.

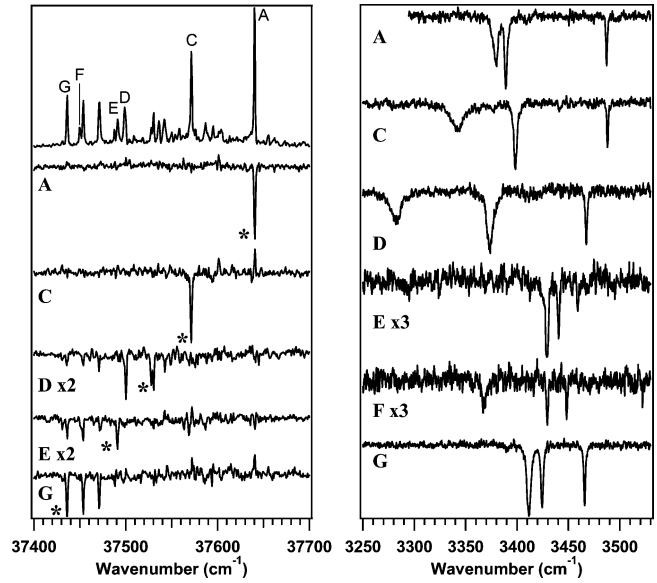


***Figure 2.*** Left Panel: R2PI spectrum of ***β*α**L (top trace) and UVHB spectra of ***β*α**L (lower traces). Asterisks show the transition on which the HB laser was fixed. The small transitions to the red of the transitions marked by an asterisk in D and E are artifacts arising from incomplete subtraction. Right Panel: RIDIR spectra of ***β*α**L.

Furthermore, to gain an additional point of comparison between experiment and theory, vertical excitation energies were computed using single point time-dependent density functional theory (TD-DFT) calculations at the B3LYP/6-31+G(d) level of theory for a selected subset of the B3LYP/6-31+G(d) optimized ground-state geometries found within the first 30 kJ/mol for ***β*α**L, ***β*α**D, and **α*β***L.

## 3. Results

**3.1. Conformation-Specific Spectroscopy. 3.1.1. Ac-$\beta^3$-hAla-L-Phe-NHMe (*β*αL).** The R2PI spectrum in the $S_0-S_1$ origin region of Ac-$\beta^3$-hAla-L-Phe-NHMe (37400−37700 $cm^{-1}$) is shown in Figure 1a). The spectrum has two dominant transitions (labeled A and C at 37647 and 37578 $cm^{-1}$, respectively), and a spectrally congested region containing many weaker transitions spanning the 37400−37550 $cm^{-1}$ region. The pattern of transitions strongly suggests that several conformational isomers of ***β*α**L contribute to the spectrum.

The left panel in Figure 2 shows a set of five UVHB spectra recorded with the UV hole-burning laser fixed on the transitions marked with an asterisk. These hole-burning spectra account for all transitions observed in the spectrum of ***β*α** apart from the weak shoulder in the R2PI trace labeled 'F'. As we shall see, transition 'F' can also be assigned to a conformer of ***β*α**L due to its unique infrared spectrum. One can conclude, therefore, that diastereomer ***β*α**L divides its population among six conformational isomers, with $S_0-S_1$ origins at 37647 (A), 37578 (C), 37504 (D), 37498 (E), 37457 (F), and 37443 $cm^{-1}$ (G). The UVHB spectra of the two dominant conformers A and C and the minor conformer E are single transitions in the origin region, indicating little change in their geometry along the low-frequency torsional modes upon electronic excitation ($\Delta v = 0$ Franck−Condon factors). On the other hand, conformers D and G show, in addition to origin transitions, significant low-frequency vibronic activity, indicating a stronger interaction of the phenyl ring with the peptide backbone responsible for the low-frequency modes in the molecule.

To gain additional insight into the structure of these six conformers of ***β*α**L, conformation-specific infrared spectra were recorded using RIDIR spectroscopy. The right panel of Figure 2 shows these scans over the 3250−3530 $cm^{-1}$ region where the NH stretch fundamentals are anticipated to occur. In the absence of H-bonding, the amide NH stretch fundamentals occur in the 3450−3500 $cm^{-1}$ region.[13,63−67] Intramolecular H-bonds shift the NH stretch to lower wavenumbers, increase its intensity, and often lead to measurable broadening relative to their non-H-bonded counterparts.[68] On this basis, we see that conformers A, C, and D show similar patterns, with each containing a single sharp transition above 3450 $cm^{-1}$ ascribable to a free amide NH stretch, and two broad, intense transitions shifted below 3400 $cm^{-1}$, indicative of two H-bonded NH groups. The spectral

(57) van Mourik, T. *J. Chem. Theory Comput.* **2008**, *4*, 1610.
(58) White, B. R.; Wagner, C. R.; Truhlar, D. G.; Amin, E. A. *J. Chem. Theory Comput.* **2008**, *4*, 1718.
(59) Zhao, Y.; Truhlar, D. G. *J. Chem. Theory Comput.* **2005**, *1*, 415.
(60) Zhao, Y.; Truhlar, D. G. *Acc. Chem. Res.* **2008**, *41*, 157.
(61) Dooley, R.; Allen, G.; Pamidighantam, S. *Proceedings of the 13th Annual Mardi Gras Conference*; Computational Chemistry Grid: Production Cyberinfrastructure for Computation Chemistry, Baton Rouge, LA, U.S.A., 2005, Baton Rouge.
(62) Milfeld, K.; Guiang, C.; Pamidighantam, S.; Giuliani, J. Cluster Computing through an Application-Oriented Computational Chemistry Grid, *Proceedings of the 6th Linux Clusters Institute Conference*, The HPC Revolution, Chapel Hill, NC, April 25-28, 2005; http://www.linuxclustersinstitute.org/conferences/archive/2005/PDF/23-Milfeld_K.pdf.
(63) Fricke, H.; Funk, A.; Schrader, T.; Gerhards, M. *J. Am. Chem. Soc.* **2008**, *130*, 4692.
(64) Fricke, H.; Gerlach, A.; Unterberg, C.; Rzepecki, P.; Schrader, T.; Gerhards, M. *Phys. Chem. Chem. Phys.* **2004**, *6*, 4636.
(65) Fricke, H.; Schafer, G.; Schrader, T.; Gerhards, M. *Phys. Chem. Chem. Phys.* **2007**, *9*, 4592.
(66) Gerlach, A.; Unterberg, C.; Fricke, H.; Gerhards, M. *Mol. Phys.* **2005**, *103*, 1521.
(67) Unterberg, C.; Gerlach, A.; Schrader, T.; Gerhards, M. *J. Chem. Phys.* **2003**, *118*, 8296.
(68) Pimentel, G. C.; McClellan, A. L. *The Hydrogen Bond*; W. H. Freeman: San Francisco, 1960.

***Table 1.*** Experimentally Determined $S_0-S_1$ Origin Transition Frequencies and Intensities, and Amide NH Stretch IR Transitions for the Conformers of **βαL**, **βαD**, and **αβL**; also Included Are Assigned Conformational Families, Specific Structural Assignments, and Diastereomeric Pairings (**βαL** and **βαD**)

| conformer | intensity | conformational family | assignment | expt $S_0-S_1$ origin ($cm^{-1}$) | expt. NH stretches ($cm^{-1}$) | | | diastereomeric parings |
|---|---|---|---|---|---|---|---|---|
| **βαL**(A) | strong | C8/C7 | C8c/$C7_{eq}(a)$ | 37647 | 3380 | 3389 | 3487 | **βαD**(A′) |
| **βαL**(C) | strong | C8/C7 | C8a/$C7_{eq}(g_-)$ | 37578 | 3342 | 3398 | 3488 | **βαD**(C′) |
| **βαL**(D) | medium | C8/C7 | C8b′/$C7_{eq}(g_-)$ | 37504 | 3282 | 3374 | 3467 | *a* |
| **βαL**(E) | weak | C5, C6/C5, or $C7_{eq}$ | − | 37498 | 3428 | 3440 | 3459 | − |
| **βαL**(F) | weak | C11, $C7_{eq}$, or C6/$C7_{eq}$ | − | 37457 | 3367 | 3429 | 3448 | − |
| **βαL**(G) | strong | C6/C5 | C6b/C5(*a*) | 37443 | 3411 | 3424 | 3466 | **βαD**(G′) |
| **βαD**(A′) | strong | C8/C7 | C8d/$C7_{eq}(g_-)$ | 37647 | 3373 | 3385 | 3469 | **βαL**(A) |
| **βαD**(B) | strong | C11 | C11($g_+$) | 37593 | 3389 | 3435 | 3448 | − |
| **βαD**(C′) | strong | C8/C7 | C8a/$C7_{eq}(a)$ | 37575 | 3331 | 3357 | 3462 | **βαL**(C) |
| **βαD**(X) | weak | C8/C7 | C8a/$C7_{eq}(a)$ | 37571 | 3321 | 3365 | 3475 | − |
| **βαD**(G′) | weak | C6/C5 | C6b/C5($g_-$) | 37437 | 3396 | 3411 | 3451 | **βαL**(G) |
| **βαD**(Y) | weak | C8/C7 | C8b/$C7_{eq}(g_-)$ | 37651 | 3293 | 3390 | 3455 | *a* |
| **αβL**(A) | strong | C5/C8 | C5/C8b(*a*) | 37412 | 3388 | 3418 | 3448 | − |
| **αβL**(B) | strong | C5/C6 | C5/C6a(*a*) | 37231 | 3402 | 3447 | 3500 | − |
| **αβL**(C) | weak | $C7_{eq}$, or C7/C11 | − | 37508 | 3274 | 3436 | 3440 | − |
| **αβL**(D) | weak | C7/C8 | $C7_{eq}$/C8b($g_+$) | 37642 | 3314 | 3399 | 3464 | − |
| **αβL**(E) | weak | C5/C6 | C5/C6a($g_-$) | 37533 | 3400 | 3444 | 3498 | − |
| **αβL**(F) | weak | C11 or C5 | − | 37525 | 3440 | 3444 | 3467 | − |

[a] While **βαL**(D) and **βαD**(Y) are assigned to C8b/$C7_{eq}(g_-)$, both have the aromatic ring in position ($g_-$) and so do not form a diastereomeric pair (see text for further discussion).

signature of conformer G shares the same pattern of one free and two H-bonded NH stretch transitions; however, the shifts of the latter two transitions are significantly less, indicating weaker H-bonds. The minor conformer E has all three of its NH stretch fundamentals above 3400 $cm^{-1}$, with an intensity pattern suggesting one weak H-bond and two free NH groups. Finally, the other minor conformer F has one strong H-bond, and two free or weakly H-bonded NH groups.

The experimental intensities, $S_0-S_1$ origin positions, and NH stretch infrared fundamentals for individual conformations of **βαL** are summarized in Table 1. Also included in the table are the assignments to particular conformational families made based on the comparison with calculation, which is not taken up in detail until section 3.2.2.

**3.1.2. Ac-$\beta^3$-hAla-D-Phe-NHMe (βαD).** Figure 1b) presents the R2PI spectrum of **βαD**, shown on the same scale as that for its diastereomer **βαL** in order to facilitate a direct comparison between the two. It is clear from this comparison that the two diastereomers have distinct UV spectra easily resolved from one another under these jet-cooled conditions. The left panel of Figure 3 reproduces this same R2PI spectrum (top trace), with the set of UVHB spectra shown immediately below it. The transitions assigned to conformer B of **βαD** have no close analogue in **βαL**, indicating that this conformer has no close diastereomeric counterpart. Some of the other features in the R2PI spectrum of **βαD** closely resemble transitions in the **βαL** spectrum; for instance, transitions A′, C′, and G′ in **βαD** are within a few $cm^{-1}$ of those for A, C, and G of **βαL**. However, in other ways, the spectrum of **βαD** is quite different than **βαL**, with most of the strong transitions in **βαD** in the 37550−37700 $cm^{-1}$ region, with very little structure present at lower wavenumber.

The UVHB spectra of the four transitions A′, B, C′, and X prove that each of these transitions are $S_0-S_1$ origins due to distinct conformers of **βαD**, located at 37647, 37593, 37575, and 37571 $cm^{-1}$, respectively (Table 1). Of these, only conformer B has significant low-frequency vibronic activity, in a progression with spacing 14 $cm^{-1}$. Transitions Y and G′ (located at 37651 and 37437 $cm^{-1}$, respectively) did not burn out with any of these four conformers.

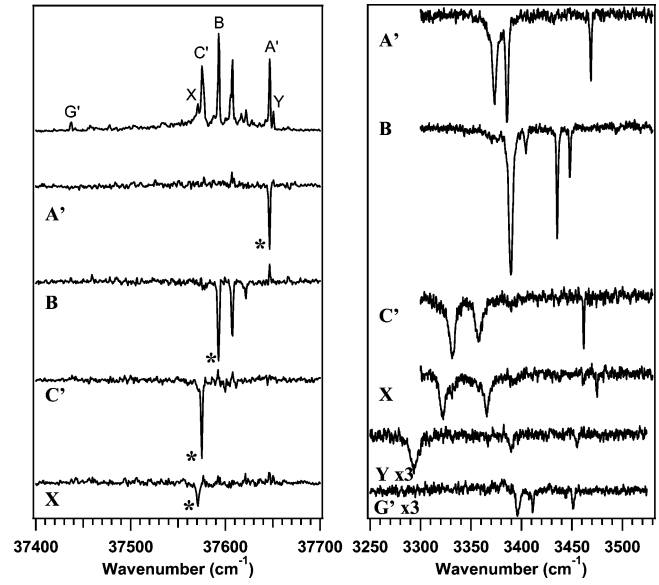


***Figure 3.*** Left Panel: R2PI spectrum of **βαD** (top trace) and UVHB spectra of **βαD** (lower traces). Asterisks show the transition on which the HB laser was fixed. Right Panel: RIDIR spectra of **βαD**.

The right panel of Figure 3 shows a series of six RIDIR spectra in the amide NH stretch region while monitoring transitions A′, B, C′, X, Y, and G′. The unique infrared spectra of transitions Y and G′ prove that these two transitions are $S_0-S_1$ origin transitions of two further minor conformers of **βαD**, bringing the total to six. The RIDIR spectra of conformers A′, C′, X, and Y reflect the presence of two intramolecular H-bonds of significant strength, with two NH stretch fundamentals below 3400 $cm^{-1}$. The spectrum of conformer B has a distinct pattern with one H-bond, and two sharp transitions suggesting free NH groups, which are nevertheless lower in wavenumber (3435, 3448 $cm^{-1}$) than most of their counterparts in the doubly H-bonded structures. Finally, conformer G′ has all three of its NH stretch fundamentals at or above 3400 $cm^{-1}$ (3396, 3411, 3451 $cm^{-1}$), in a pattern similar to that found in G (3411, 3424, 3466), but with each of the transitions shifted down by about 15 $cm^{-1}$.

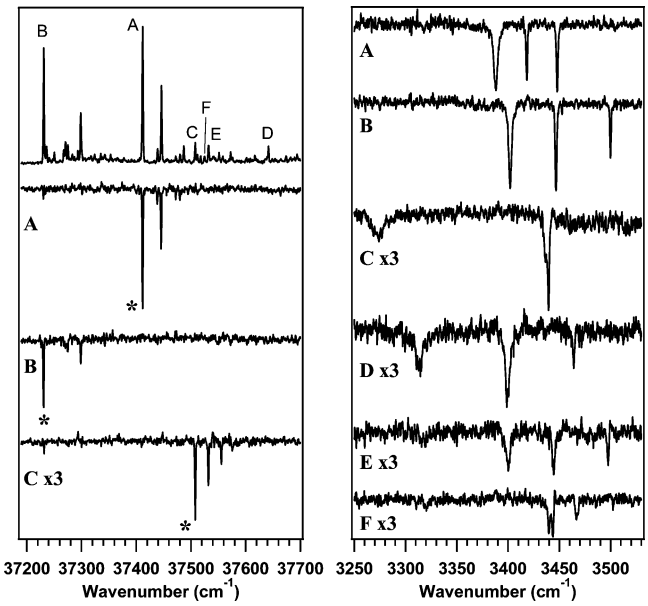


***Figure 4.*** Left Panel: R2PI spectrum of **αβL** (top trace) and UVHB spectra of **αβL** (lower traces). Asterisks show the transition on which the HB laser was fixed. Right Panel: RIDIR spectra of **αβL**.

A comparison of the UV and IR spectra of the six conformers of **βαD** with those in **βαL** reveal some natural pairings. For instance, the RIDIR spectra of A′ and C′ of **βαD** are distinct from, but closely similar to, those of A and C of **βαL**, respectively. Thus, these conformers are nearly identical both in their UV and IR spectra, strongly suggesting that A/A′ and C/C′ are each diastereomer pairs that are affected little by the chirality change at the Phe position. Similarly, **βαD**(G′) has its $S_0-S_1$ origin transition within a few $cm^{-1}$ of **βαL**(G), and both share similar IR spectral patterns, suggesting that these two also belong to the same conformational family with similar H-bonds (reflected in the IR spectra) and similar interactions of the Phe side chain (which is responsible for the UV absorption), with the α-peptide subunit of which it is a part.

Within the six conformers of **βαD** there are also natural pairings to be made. In the UVHB spectra of Figure 3, transition Y appears within a few $cm^{-1}$ of A′, while X is a similar shift from C′, suggesting that A′/Y and C′/X are two pairs in which the phenyl ring position and its local structural environment are nearly identical. The RIDIR spectra, particularly of the latter pair, are also closely similar.

**3.1.3. Ac-;-Phe-β³-hAla-NHMe (αβL).** In an effort to understand the effect of the order of α and β subunits in α/β-peptides, we have carried out single-conformation spectroscopy on Ac-L-Phe-β³-hAla-NHMe (**αβL**) to compare with Ac-β³-hAla-L-Phe-NHMe (**βαL**). Note that the phenylalanine side chain remains on the α-peptide unit.

The left panel of Figure 4 shows the R2PI and UVHB spectra of three conformers resolved with these methods. The R2PI spectrum in the origin region, 37200−37700 $cm^{-1}$, (top trace) reveals two dominant transitions, labeled A (37412 $cm^{-1}$) and B (37231 $cm^{-1}$), separated by 181 $cm^{-1}$. UVHB spectra with hole-burning laser fixed on transitions A and B, respectively, prove that these transitions are $S_0-S_1$ origin transitions of two dominant conformers of **αβL** (Table 1). Several additional transitions on the blue edge of the R2PI spectrum do not burn with either of these bands. When transition C was used as hole-burning transition, the UVHB spectrum at the bottom of Figure 4 resulted, revealing the spectrum of a minor conformer with $S_0-S_1$ origin located at 37508 $cm^{-1}$. Due to their comparative weakness, remaining transitions not identified by these UVHB spectra were identified as distinct conformations via their unique infrared spectra.

Figure 4 (left panel) shows RIDIR spectra due to six resolved conformers of **αβL** the three conformers already identified by UVHB (conformers A−C), and three others labeled in the R2PI spectrum at the top of Figure 4 as D−F. The RIDIR spectra of the six conformers of **αβL** have quite different patterns from one another, indicating that up to five distinct intramolecular H-bonding arrangements are present. Only the major conformer B and the minor conformer E show a close resemblance. These two conformers, unlike all others, have a free NH stretch near 3500 $cm^{-1}$, some 30−40 $cm^{-1}$ higher than the other four conformers. In the β-peptide analogues studied previously by our group (Ac-β³-hPhe-NHMe, Ac-β³-hPhe-β³-hAla-NHMe, and Ac-β³-hAla-β³-hPhe-NHMe),[8,9] the NH stretch fundamental of the free terminal NH group (NHMe) in the β-peptides occurs consistently in the 3490−3500 $cm^{-1}$ range, while the free NH stretch of the interior branched-chain NH groups were approximately 30−40 $cm^{-1}$ lower in frequency. Based on the work of Marraud in solution, this shift is known to be a general feature of β-peptide NH groups.[69] On this basis, we surmise that the terminal NHMe is free in **βαD**(B) and **βαD**(E), but not in the others.

The two dominant conformers of **αβL** (A and B) have all their NH stretch fundamentals near to or above 3400 $cm^{-1}$ (Figure 4, right and Table 1), in striking contrast to the dominant conformers of its counterpart **βαL** for which three of the four major conformers (A, C, D in Figure 3) have one or more absorptions well below 3400 $cm^{-1}$. Thus, the conformers with large population in **αβL** are different than those in **βαL**. The minor conformer **αβL**(D) has a spectrum analogous in its spacing and intensity patterns to that of **βαL**(D), suggesting that the two belong to the same conformational family. The other minor conformers **αβL**(C) and **αβL**(F) are quite unique, with the former having no analogue in other spectra, and that of **αβL**(F) somewhat similar in pattern to that of **βαL**(E).

**3.2. Calculations.** To gain further insight to the preferred conformations and their spectral signatures and to provide a direct comparison with experiment, *ab initio* and DFT calculations were carried out on **βαL**, **βαD** and **αβL**. These calculations build on previous computational work on model β-peptides and α/β-peptides similar to those studied here.[70,71]

**3.2.1. Structures and Relative Energies of Conformational Minima.** Full optimizations of 118 structures of **βαL**, 65 structures of **βαD**, and 81 structures of **αβL** were carried out at the DFT B3LYP/6-31+G(d) level of theory. In order to account for the fact that DFT B3LYP/6-31+G(d) calculations do not properly account for dispersive interactions, single-point energy calculations at the MP2/6-31+G(d) level of theory, which explicitly account for electron correlation effects, were computed for all minima found at the DFT B3LYP/6-31+G(d). Since MP2/6-31+G(d) calculations suffer from large intramolecular basis set superposition error,[52,53] we have also computed a subset of relevant minima using Truhlar's density functional

(69) Marraud, M.; Neel, J. *J. Polym. Sci.* **1975**, 271.
(70) Mohle, K.; Gunther, R.; Thormann, M.; Sewald, N.; Hofmann, H. J. *Biopolymers* **1999**, *50*, 167.
(71) Wu, Y. D.; Han, W.; Wang, D. P.; Gao, Y.; Zhao, Y. L. *Acc. Chem. Res.* **2008**, *41*, 1418.

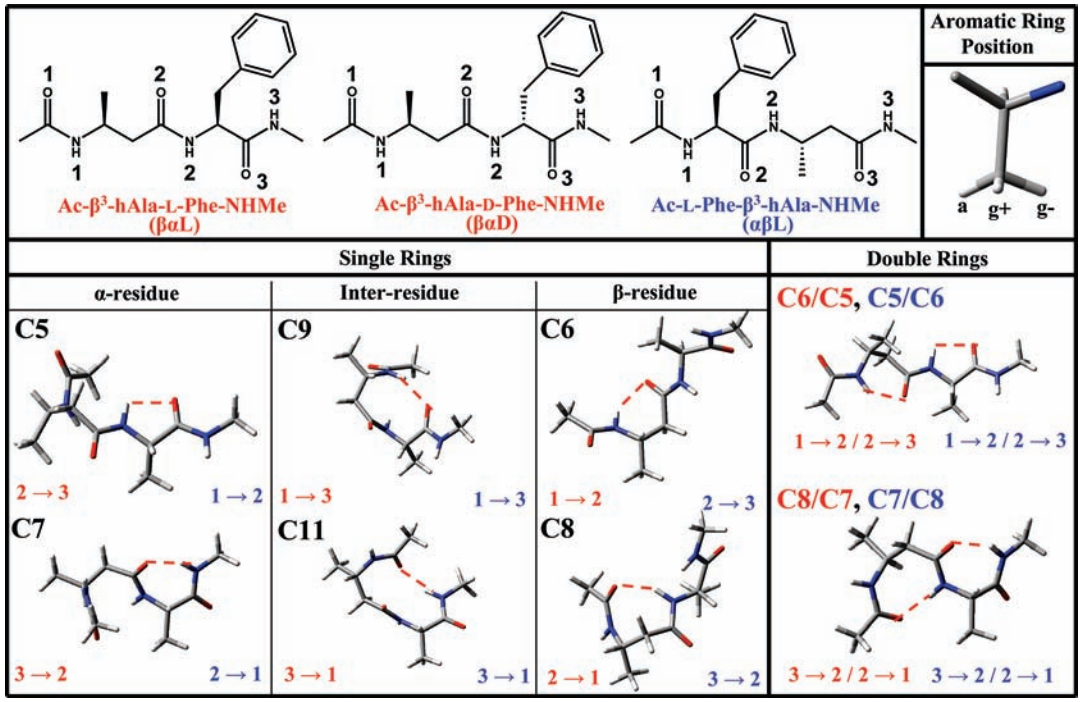


***Figure 5.*** Representative peptide backbone structures, arranged by H-bonding architecture with the phenyl ring removed for clarity. (Right/Top) Structures for **βαL**, **βαD**, **αβL** with the amide labeling scheme N-terminus (1), Middle (2), and C-terminus (3) shown for **βαL**. (Left/Top) Three possible positions for the phenyl chromophore, where the *a*, *g*+, and *g*- follows the form of refs.[10−12] (Left/Bottom) Possible single ring H-bonding architectures arranged by the residue forming the H-bond α-residue (C5, C7), inter-residue (C9, C11), and *β*-residue (C6, C8). (Right/Bottom) Sequential double ring structures C6/C5, C5/C6, C8/C7, and C7/C8. In addition to the H-bond ring labels, numeric labeling is included showing the amide NH and C=O involved in the H-bond, where the amide NH precedes the C=O.

M05-2X with the 6-31+G(d) basis set, which was developed to better account for dispersive interactions.[49]

As anticipated, the conformational minima can be placed into conformational 'families' based on unique intramolecular H-bonding arrangements of the peptide backbone. These can be characterized principally by the number and type of H-bonded rings involved. In referring to these structures, we will identify them as single-ring or double-ring structures, and label them by the size of the H-bonded rings present. For example, a C8/C7 double-ring structure has one 8-membered H-bonded ring and one 7-membered ring.

Figures 5 and 6 provide examples of these peptide backbone arrangements, where the phenyl ring has been replaced by a hydrogen atom in order to highlight the peptide backbone conformation. For each of the three molecules **βαL**, **βαD**, and **αβL**, there are six possible single-ring hydrogen bonding motifs involving interamide NH···O=C H-bonds, classified by the residue on which they occur, α-, *β*-, or inter-residue. As anticipated, rings involving the α-residue form odd-membered rings (C5, C7), the *β*-residue even-membered rings (C6, C8), and the inter-residue structures larger odd-membered rings (C9, C11). The chemical structures on the top of the figure have amide groups labeled 1−3, beginning from the N-terminus. Elsewhere in the figure, the *x*→*y* labeling indicates the H-bonding arrangement involved, with the number of the amide NH first (which acts as H-bond donor) and the C=O acceptor second. Following this convention, if either diastereomer of **βα** were to form a single C7 cycle, it would be labeled 3 → 2, while a C7 of **αβL** would be labeled 2 → 1. Since the molecules **αβ** and **βα** differ in the order of the α and *β*-residues, the double-ring structures have different ordering of the H-bonded rings, which are not equivalent. Thus, **βα** has C6/C5 and C8/C7 double rings, while the **αβ** has C5/C6 and C7/C8. The single-ring and double-ring structures shown in the figure have the backbone appropriate for **βα**.

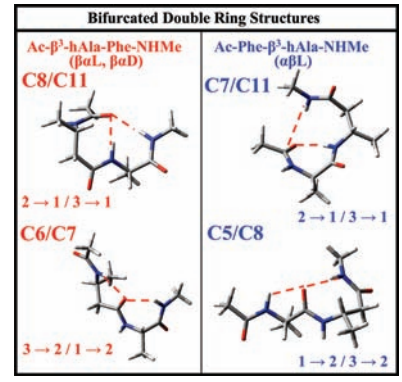


***Figure 6.*** Representative peptide backbones for the bifurcated double-ring structures, arranged by H-bonding architecture with the phenyl ring removed for clarity. Bifurcated double-ring structures formed in **βαL** and **βαD** (Right Panel) and **αβL** (Left Panel). In addition to the H-bond ring labels, numeric labeling is included showing the amide NH and C=O involved in the H-bond, where the amide NH precedes the C=O. Structures using C=O(3) as an acceptor are not formed presumably due to steric hindrance (see text).

The structures shown in Figure 6 are bifurcated double-ring structures, in which the two H-bonded rings involve different amide NH groups donating H-bonds to the same acceptor C=O, making use of the two lone pairs of electrons on the carbonyl oxygen. In this case, the different ordering of α- and *β*-residues in **βα** and **αβ** produce different H-bonded ring sizes, with the central carbonyl accommodating H-bonds to form C7/C6 double rings in **βα** and C5/C8 double rings in **αβ**. Similarly, when the acetyl carbonyl 1 accepts H-bonds from amide NH groups 2 and 3, it forms a C8/C11 double ring in **βα**, but a C7/C11

double-ring in **αβ**. Bifurcated double-ring structures involving carbonyl 3 as acceptor (C5/C9 in **βαL** and C9/C6 in **αβL**) do not produce stable minima, presumably due to steric hindrance.

In all but the C5 ring, it is possible to form a given H-bonded ring size with different sets of dihedral angles involving the atoms that comprise the ring. This leads to subfamilies of structures that share a given set of dihedral angles, structures for which are shown in the Supporting Information (Figure S1). Both the C6 and C7 rings come in two types, in which the substituted chiral side chain takes up an axial or equatorial position relative to the nominal plane of the $C_n$ ring.[10,25,30,70] In the C6 rings, we label these types C6a (axial) and C6b (equatorial), while in the C7 rings we explicitly mention the axial or equatorial position ($C7_{ax}$ and $C7_{eq}$) to maintain continuity with previous work on α-peptides.[10,11,14,29,72] Comparison of the relative energies calculated for similar structures that differ only in the C6 ring type predict that the two are similar in energy, at times swapping energy ordering, depending on the level of theory used. Previous studies on α-peptides have observed a clear preference for $C7_{eq}$ structures, which are calculated to be ~10 kJ/mol more stable than $C7_{ax}$.[10,25,30] This same preference appears to carry over to the α/β-peptides. There are four energetically preferred C8 rings (C8a, C8b, C8c, C8d), which are close enough in energy that other factors (e.g., a second H-bonded ring or NH···π interaction) can reverse their relative stabilities.

The number of independent dihedral angles in a H-bonded ring grows with ring size. While the constraints imposed by bringing the two ends of the molecule together limit the number of possibilities, the number of independent ring-types becomes quite large with C9 and C11. For instance, among the C11 structures of **βαL** in the first 30 kJ/mol at the single-point MP2/6-31+G(d) level, we have identified 10 distinct types of C11 ring. Table S1 (Supporting Information) connects a letter label with a given set of dihedral angles for each Cn ring size. The double-ring structures incorporate these different ring subtypes, leading to a large number of double-ring structures with H-bonds involving a range of NH···O=C H-bond distances, approach angles, and degrees of cooperative strengthening.

Finally, there exist three possible positions for the aromatic ring for each type of peptide backbone structure, based on the three possible staggered torsion angle about the bond between the backbone carbon and the side chain methylene carbon that is connected to the ring. The three possible positions for the aromatic ring are shown in Figure 5, labeled as (*a*), ($g_+$), and ($g_-$), in keeping with the scheme used by Mons and co-workers.[12,33] For example, a C6b ring with the chromophore in position (*a*) is denoted C6b(*a*). The position of the aromatic ring plays an important role in providing additional stabilization to certain structures, particularly when the formation of an NH···π H-bond is possible. Alternatively, specific aromatic ring positions of a particular structural motif may be disfavored because of steric hindrance (e.g., position ($g_-$) of C5/C8 double ring/double acceptor structures).

The Supporting Information (Table S2) presents zero-point corrected relative energies of all structures of **βαL** within 30 kJ/mol of the global minimum, and a representative subset of structures of **βαD** and **αβL**, calculated at the DFT B3LYP/6-31+G(d) and single-point MP2/6-31+G(d) levels of theory. DFT M05-2X/6-31+G(d) calculations were also carried out on a subset of structures of all three molecules. Figure 7 presents schematic energy level diagrams for the conformational isomers of **βαL**, **βαD**, and **αβL**, summarizing the results at the three levels of theory. The structures are divided into the main conformational families present, with all other structures gathered into a single column to the right.

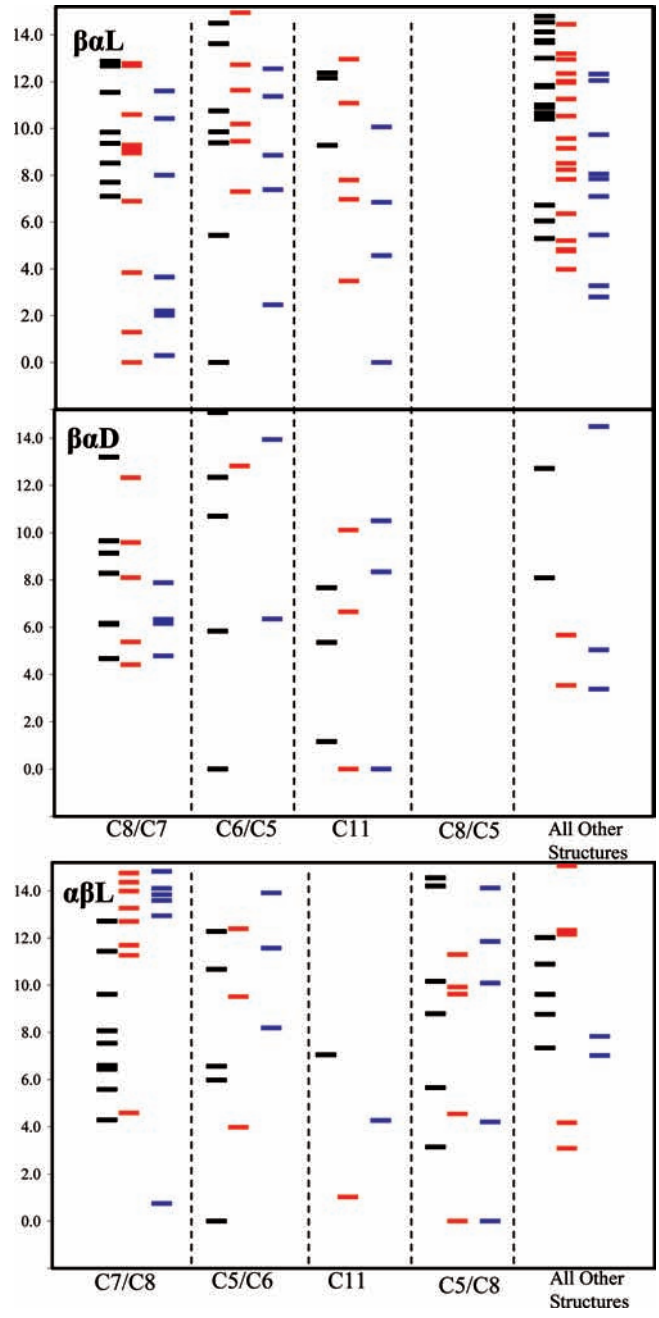


***Figure 7.*** Energy level diagrams for all structures of **βαL** (top), and a subset of structures of **βαD** (middle), and **αβL** (bottom) found within the first 15 kJ/mol as calculated by B3LYP/6-31+G(d). The energy levels are divided into the major conformational families observed. Black lines correspond to zero-point corrected B3LYP/6-31+G(d) energies, red lines are single-point MP2/6-31+G(d) energies at the B3LYP/6-31+G(d) optimized geometries, and blue lines show a subset of the B3LYP/6-31+G(d) structures optimized at the M05-2X/6-31+G(d) level of theory. All three include zero-point corrections at the B3LYP/6-31+G(d) level of theory.

Not surprisingly, there are systematic differences in relative energies of structures belonging to the main families when computed at the different levels of theory. A detailed analysis

(72) Dian, B. C.; Longarte, A.; Mercier, S.; Evans, D.; Wales, D. J.; Zwier, T. S. *J. Chem. Phys.* **2002**, *117*, 10688.

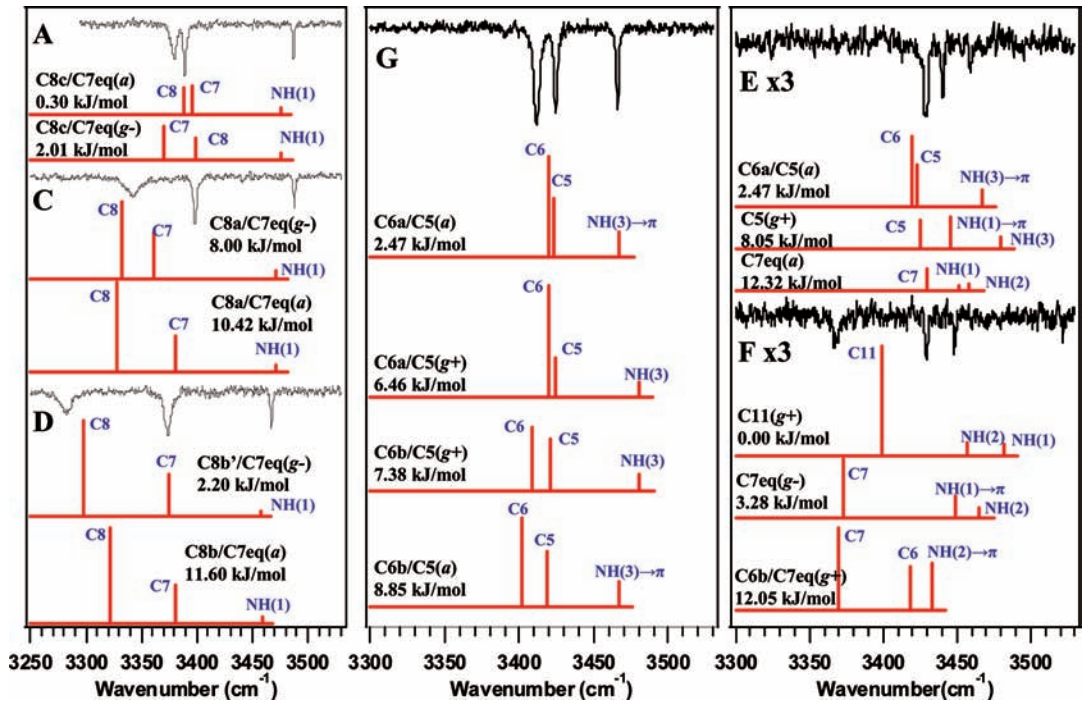


***Figure 8.*** Experimental amide NH stretch RIDIR (black traces) and calculated, scaled (0.96) harmonic vibrational frequency and infrared intensity stick diagrams (red traces) with normal mode description (blue labels) at the B3LYP/6-31+G(d) level of theory for the six conformers of ***βαL***. Also included for ready comparison are M05-2X/6-31+G(d) energies. Left Panel: Conformers ***βαL***(A), ***βαL***(C), ***βαL***(D) and representative best-fit C8/C7 stick spectra. Middle Panel: RIDIR spectra of conformer ***βαL***(G) and representative C6/C5 stick spectra. Right Panel: RIDIR spectra of conformers ***βαL***(E) and ***βαL***(F) and representative stick spectra.

of these differences is beyond the scope of this paper. On the basis of previous work, we anticipate that the DFT M05-2X calculations represent a reasonable compromise between the DFT B3LYP calculations, which systematically underestimate dispersion,[50−53,57] and MP2 calculations, which overestimate dispersion and suffer from large basis set superposition error.[52,53] This is reflected in a preference for extended structures (e.g., C6/C5) over more compact double-ring or large single-ring structures (C8/C7 and C11) in DFT B3LYP, which is reversed in the MP2 calculations. The DFT M05-2X calculations predict relative energies somewhere between these two extremes.

While none of these levels of theory is definitive, they do show trends that deserve discussion. First, the lowest-energy members of the main conformational families in most cases have energies within 5 kJ/mol of one another. This suggests the possibility that these main families may be represented among the observed conformers of all three molecules. Second, while in ***βαL***, C8/C7 and C11 structures are comparable in energy, in ***βαD***, all three levels of theory predict the presence of a very low-energy C11 structure that is the global minimum at the MP2 and DFT M05-2X levels of theory. Third, in the ***αβL*** (Figure 7), the same two levels of theory predict a C5/C8 bifurcated double-ring structure as its global minimum. This structure, which uses the central C=O as double acceptor site, becomes the C7/C6 structure in ***βαL*** and ***βαD***, and is thereby pushed up in energy significantly, relative to other double-ring structures (e.g., C7/C8). While the C5 structure does not produce a strong H-bond, it does stabilize the C5/C8 structure in ***αβL*** considerably, relative to a C8 single-ring structure in which the NH(1) is rotated away from C=O(2).

**3.2.2. Vibrational Frequencies, Infrared Intensities, and $S_0-S_1$ Energy Separations: Comparison with Experiment.** Harmonic vibrational frequencies and infrared intensities were calculated for all optimized structures within 30 kJ/mol of the global minimum for ***βαL***, ***βαD***, and ***αβL***, using DFT B3LYP/6-31+G(d). The primary point of comparison with experiment here is the amide NH stretch region. Figures 8− 10 compare the observed RIDIR spectra for ***βαL***, ***βαD***, and ***αβL***, respectively, with calculated harmonic vibrational frequencies and infrared intensities at this level of theory, scaled with a scale factor of 0.96, a value chosen to match the experimental free amide NH stretch of the free amide NH group. In each case, calculated stick spectra that best match a given conformation-specific RIDIR spectrum are shown immediately below the experimental spectrum. The fact that more than one calculated structure is associated with a given observed structure makes clear that, while the comparison enables us to assign specific conformers as members of particular conformational families, it is not always possible to assign them to specific single conformational isomers with certainty.

The position of the $S_0-S_1$ origins of the conformers in the R2PI spectrum provides another point of comparison with theory. Single-point TDDFT B3LYP/6-31+G(d) calculations at the DFT B3LYP/6-31+G(d) optimized ground-state geometry have been carried out on a subset of the low-energy structures of ***βαL***, ***βαD***, and ***αβL***. We would anticipate that the $S_0-S_1$ origin to be most sensitive to the local α-peptide conformation (C5, $C7_{eq}$, $C7_{ax}$) to which it is attached, and to the position of the phenyl ring. On the basis of the studies of Mons and co-workers on the α-peptide analogues,[11] it is known that the $S_0-S_1$ origins of C5 conformers are typically shifted to the red, relative to the $C7_{eq}$ conformers ($C7(\gamma_L)$). We would anticipate this same shift to hold here, which we will see shortly it does. While the absolute separations predicted by TDDFT are significantly too high, the wavenumber shifts with conformation and between the ***βαL***, ***βαD***, and ***αβL*** structures can be used as another test

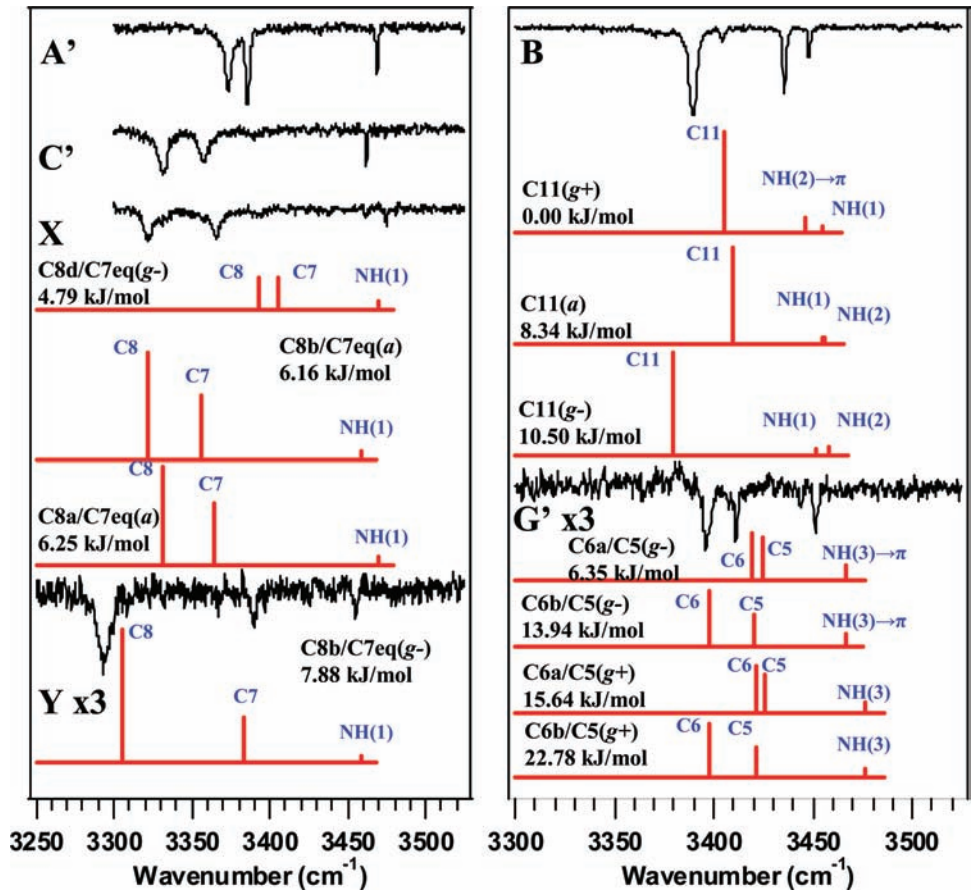


***Figure 9.*** Experimental amide NH stretch RIDIR (black traces) and calculated, scaled (0.96) harmonic vibrational frequency and infrared intensity stick diagrams (red traces) with normal mode description (blue labels) at the B3LYP/6-31+G(d) level of theory for the six conformers of **βαD**. Also included for ready comparison are M05-2X/6-31+G(d) energies. Left Panel: Conformers **βαD**(A′), **βαD**(C′), **βαD**(X), **βαD**(Y) and representative best-fit C8/C7 stick spectra. Right Panel: RIDIR spectra of conformers **βαD**(B) and **βαD**(G) and representative stick spectra.

of the assignments to specific conformational families or specific subfamily structures. Table S3 in the Supporting Information contains the TDDFT predictions for the shifts in the vertical excitation energies relative to the vertical excitation energy of **βαL**(A),

$$\Delta E_{\mathrm{vert}}^{\mathrm{rel}}(S_0 - S_1)$$

, a strong, firmly assigned structure with $S_0-S_1$ origin as far blue-shifted as any observed.

**3.2.2.1. Ac-$\beta^3$-hAla-L-Phe-NHMe (βαL).** The left panel of Figure 8 contains the experimental NH stretch RIDIR scans of conformers A, C, and D of the **βαL** diastereomer Ac -$\beta^3$-hAla-L-Phe-NHMe. These spectra share a similar spectral pattern, containing two H-bonded and one free amide NH stretch. However, they differ quite substantially in the wavenumber positions and relative intensities of the H-bonded NH stretch fundamentals, particularly the lowest wavenumber transition. As the calculated 'best-fit' stick spectra show, the three conformers A, C, and D are all assigned as C8/$C7_{eq}$ double-ring structures, differing in the type of C8 ring involved. One of the structures which was a plausible fit to the RIDIR spectrum of conformer C was a C8c/$C7_{ax}$ structure (not shown). However, the calculated positions of the $S_0-S_1$ origins of C8/$C7_{ax}$ structures are predicted to be red-shifted (Table S3, Supporting Information) by about 1000 $cm^{-1}$ relative to C8/$C7_{eq}$, counter to observation. Thus, we focus attention on the C8/$C7_{eq}$ double rings as candidate structures. These structures produce only modest shifts in the NH stretch fundamental involved in the C7 H-bond, which is the higher wavenumber of the two H-bonded NH stretch transitions in all but one of the calculated structures (C8c/$C7_{eq}(g_-)$). In contrast, the best-fit structures for A, C, and D belong to different C8 subfamilies, which modulate the distance and orientation of the NH···O=C H-bond in the C8 ring quite substantially. This produces NH stretch frequencies for the lower-frequency NH stretch mode spread over almost 100 $cm^{-1}$ (3280−3380 $cm^{-1}$), leading to very different appearances for the spectra of different C8/$C7_{eq}$ structures, even though they are all nominally of the same family type.

More subtle spectral differences are associated with the position of the aromatic ring, whose presence may have a further indirect effect on the dihedral angles in the C7 or C8 rings and hence in the strength of the NH···O=C H-bonds in the two rings. One would anticipate that the C7 ring would be most sensitive to the Phe side-chain position, since the Phe side chain is appended to this ring. However, the calculations show that both amide NH stretch frequencies can be perturbed by the position of the aromatic ring.

The middle panel of Figure 8 compares the RIDIR spectrum of conformer G with four best-fit stick spectra, all of which are C6n/C5 double rings and differ in the position of the aromatic ring. On this basis, conformer G is assigned to a C6b/C5 double ring structure, and is the only highly populated conformer in the R2PI spectrum which is not a C8/C7 double ring. The two H-bonded NH stretch transitions in G are both above 3400 $cm^{-1}$, indicating weaker hydrogen bonding, as anticipated based on previous work on C5 and C6 conformers of α- and β-peptides.[8,9,11,13,14]

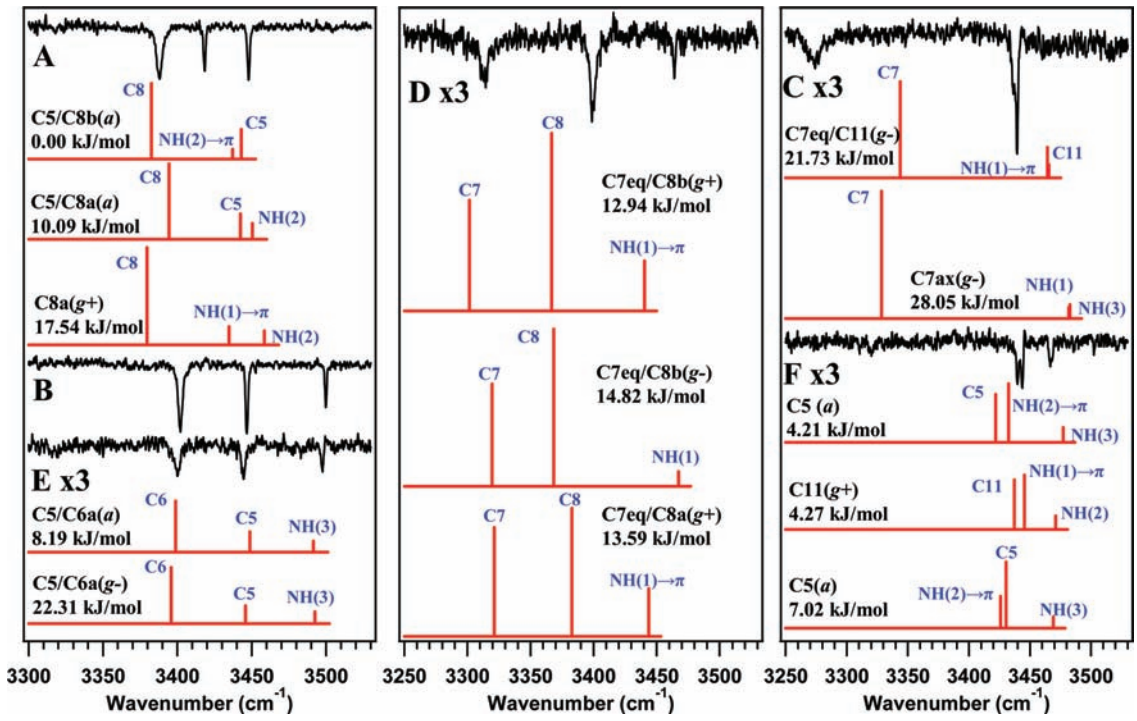


***Figure 10.*** Experimental amide NH stretch RIDIR (black traces) and calculated, scaled (0.96) harmonic vibrational frequency and infrared intensity stick diagrams (red traces) with normal mode description (blue labels) at the B3LYP/6-31+G(d) level of theory for the six conformers of **αβL**. Also included for ready comparison are M05-2X/6-31+G(d) energies. Left Panel: Conformers **αβL**(A), **αβL**(B), **αβL**(E) and representative best-fit stick spectra. Middle Panel: RIDIR spectra of conformer **αβL**(D) and representative stick spectra. Right Panel: RIDIR spectra of conformers **αβL**(C) and **αβL**(F) and representative stick spectra.

The computed stick spectra are changed only slightly in the hydrogen bonded NH stretch region; however, an NH$\cdots\pi$ interaction found in the C6b/C5($a$) structure causes a shift to lower wavenumber for the free NH stretch, providing a slightly better match with experiment. This NH$\cdots\pi$ interaction is also consistent with the observed Franck−Condon progression in the UVHB spectrum (Figure 2G, left panel).

Finally, the right-hand panel of Figure 8 examines the minor conformers E and F of **βαL**. The spectral pattern for E resembles that of G, which has just been assigned to a C6/C5 double ring. Thus, it is plausible to assign E to one of the other C6n/C5 structures not taken by G (Figure 8, middle). However, by comparison to G, the three NH stretch fundamentals of E are at higher wavenumber, with only a 31 cm$^{-1}$ interval separating all three (3428, 3440, and 3459 cm$^{-1}$), arguing against a C6 H-bond and in favor of structures containing only free or very weak H-bonds. This opens the possibility that E should be assigned to a weak single-ring, with two possibilities shown in Figure 8. At present, we cannot distinguish between these with any certainty.

The RIDIR spectrum of conformer F (Figure 2F, right panel) does not have a close analogue among the other conformers of **βαL**, but does bear some resemblance to the spectrum of conformer B of the diastereomer **βαD** (Figure 3G, right panel). As we shall see, **βαD**(B) is assigned with some confidence to a C11 single-ring structure, suggesting a similar assignment for **βαL**(F). Figure 8 shows the calculated spectrum of one such C11 structure (C11($g_+$)) which reproduces the observed spectral pattern. Due to the flexibility of the C11 ring, its orientation relative to the phenyl ring can vary greatly, leading to large differences in the calculated $S_0-S_1$ separations. The C11($g_+$) structure is among those in best agreement with the experimental $S_0-S_1$ origin, near the red edge of the observed conformers. Nevertheless, our assignment of **βαL**(F) must be considered tentative, with stick spectra included in Figure 8 two other structures calculated to be low in energy, which also match the experimental RIDIR spectrum similarly well.

**3.2.2.2. Ac -$\beta^3$-hAla-D-Phe-NHMe (βαD).** The two panels of Figure 9 show the calculated and experimental spectra for the six resolved conformers of the **βαD** diastereomer, Ac-$\beta^3$-hAla-D-Phe-NHMe. As noted previously, the RIDIR spectra of A′, C′, X, and Y all contain two strong H-bonds and one free NH. The assignments just made for the conformers of **βαL** provide a good starting point regarding the conformational families present. The close correspondence between $S_0-S_1$ origin positions and RIDIR spectra of **βαD**(A′) with **βαL**(A) and **βαD**(C′) with **βαL**(C) point to similar assignments for the two, marking them as C8/C7$_{eq}$ structures. The spectra of conformers X and Y, identified in section 3.1.2 as close analogues of C′ and A′, respectively, then must also be due to C8/C7$_{eq}$ structures. The stick spectra in Figure 9 bear this out. The best match with A′ is to the stick spectrum of C8d/C7$_{eq}$($g_-$), while that for C′ and X are one or the other of the C8b/C7$_{eq}$($a$) or C8a/C7$_{eq}$($a$) pair. The large spacing between the two H-bonded NH stretch transitions in Y is best fit by the C8b/C7$_{eq}$($g_-$) structure.

These assignments are strengthened by the pairings based on the UV spectrum (the $S_0-S_1$ origin positions). Recall that Y appears as a shoulder on A′ in the R2PI spectrum, while the $S_0-S_1$ origin of X is within a few cm$^{-1}$ of the C′ transition. These pairings likely reflect similar α-peptide conformations and aromatic ring positions for the Phe side chain. In keeping with this, the best-fit structures for A′ and Y in the infrared share the C7$_{eq}$($g_-$) α-peptide conformation. Similarly, the two best-fit stick spectra for C′ and X are both C7$_{eq}$($a$) structures.

Comparisons between the diastereomers are also helpful in distinguishing between candidate structures within a given

conformational family. For instance, the near-identical positions in the UV of **βαD**(A′) with **βαL**(A) suggest near-identical diastereomer equivalents in the α-peptide substructure. This is indeed the case, with $C7_{eq}(g_-)$ in **βαD**(A′) the chiral equivalent of $C7_{eq}(a)$ in **βαL**(A). Similarly, $C7_{eq}(a)$ in **βαD**(C′) maps to $C7_{eq}(g_-)$ in **βαL**(C). Finally, the pattern of IR transitions in **βαD**(Y) most closely matches that of **βαL**(D), suggesting that the two have the same C8/C7 peptide backbone. Indeed, the best-fit structure for **βαL**(D) is C8b′/$C7_{eq}(g_-)$, while that for **βαD**(Y) is C8b/$C7_{eq}(g_-)$, its close counterpart. Since both these structures have the phenyl ring in the $g_-$ position, this pair lacks the $(a)\leftrightarrow(g_-)$ mirror image symmetry in the Phe side chain, consistent with the 147 $cm^{-1}$ difference in their $S_0-S_1$ origin positions.

The right panel of Figure 9 shows stick spectra best matching the experimental NH stretch spectra of conformers B and G′ of **βαD**. Conformer B is among the three dominant conformers of **βαD**, but its spectral pattern is clearly a single-ring structure, and not the C8/C7 or C6/C5 double rings that dominate **βαL**. The best-fit stick spectra for this spectrum are all due to C11 single-ring structures. This is in keeping with the energy lowering of the C11 conformers in **βαD** relative to **βαL** (Figure 7), in which the lowest-energy C11 conformer ($C11(g_+)$) is predicted to be the global minimum in **βαD** at both the DFT M05-2X and single-point MP2/6-31+G(d) levels of theory. As noted previously, the IR spectrum of **βαD**(B) is similar to that for **βαL**(F), suggesting an assignment to a C11 structure of that minor conformer of **βαL**. The best-fit C11 stick spectrum for **βαL**(F) is also $C11(g_+)$, the same aromatic ring position as in **βαD**(B). Since position 2 is the anti position, the aromatic ring is in a near-identical environment in this diastereomeric pair. However, this is at odds with the difference in $S_0-S_1$ origin positions (Table 1), which seems more consistent with the two conformers occupying different aromatic ring positions. Thus, there remains some uncertainty whether **βαL**(F) is a C11 structure or one of the other possibilities shown in the right panel of Figure 8.

Finally, the infrared spectrum of the minor conformer **βαD**(G′) (Figure 9) is characteristic of a C6/C5 structure, with two stick spectra below it providing reasonable matches in the infrared. Given the close experimental match in both IR and UV between **βαD**(G′) and **βαL**(G), we look for analogous peptide structures and mirror image aromatic ring positions in the two. In this case, the correspondence between the *anti* and $g_-$ aromatic ring positions in the two diastereomers makes the C6b/C5($a$) in **βαL**(G) connect with C6b/C5($g_-$) in **βαD**(G′). However, the symmetric ($g_+$) position is also represented in both best-fit possibilities, leaving uncertainty in which substructures are observed.

In summary, four of the six conformers of **βαD** are C8/$C7_{eq}$ double-ring structures that differ in the C8 ring substructure and/or the position of the aromatic ring. Conformer **βαD**(B), which possesses the most intense transition in the R2PI spectrum, is assigned to a C11 structure, a conformational family represented at most by a very minor conformer in the other diastereomer **βαL**. Finally, the sixth conformer, **βαD**(G′), is a minor population C6/C5 conformer.

**3.2.2.3. Ac-L-Phe-β³-hAla-NHMe (αβL).** Figure 10 compares the experimental and computed best-fit infrared spectra for the α/β-peptide analogue, Ac-L-Phe-β³-hAla-NHMe (**αβL**). As noted in section 3.1.3, the two dominant conformers A and B differ most notably in the free amide NH stretch region. Here, conformer **αβL**(B) has a transition near 3500 $cm^{-1}$. On the basis of a comparison with previous work on β-peptides,[8,9] we deduced that the free NH in conformer B must be a terminal NHMe in amide 3 (Figure 5, top). This is consistent with an assignment to a C5/C6 double-ring structure. The calculations confirm this expectation, matching the experimental spectral patterns with C5/C6 structures (Figure 10, bottom left panel).

By comparison, the free NH stretch in **αβL**(A) appears at 3448 $cm^{-1}$. This large shift is captured by the calculations for C5/C8 double-rings, in which the free NH is NH(2), a branched NH bonded to a branched-chain carbon atom in the β-peptide subunit. This shift has been observed in previous studies of β-peptides,[8,9,69] where it was used to distinguish between C6 and C8 rings. Furthermore, the somewhat larger shift in the H-bonded NH stretch in A relative to B is consistent with the typical ordering of NH stretch frequencies noted in the β-peptides. Thus, while the pattern of transitions, particularly due to the C5 ring, does not match experiment as well as in most other cases, the frequency of the free amide NH stretch rules out an assignment to C5/C6, and instead favors one of the C5/C8 double-ring structures. This assignment is in keeping with the prediction of the calculations that the lowest-energy structures in **αβL** are C5/C8 bifurcated double-ring structures. The fact that the calculated vibrational frequencies match less well for such a bifurcated double-ring structure is likely caused by the inability of DFT B3LYP calculations to properly account for dispersive and/or electron correlation effects in these structures containing two NH groups H-bonding to the same C=O oxygen.

The assignment of A to C5/C8 and B to C5/C6 is strengthened by the positions of their $S_0-S_1$ origins. According to the TDDFT calculations (Table S4, Supporting Information), the C5/C6a($a$) structure is unusual in bringing the C6 ring over the phenyl $\pi$ cloud, producing an $S_0-S_1$ origin well red-shifted from its position in other conformers. By comparison, the C5/C8 structures are in the region more typically expected for a C5 α-peptide unit (37400−37550 $cm^{-1}$).

The minor conformer **αβL**(E) is also assigned with confidence to a C5/C6 structure (Figure 10) by virtue of its near-identical IR spectrum with **αβL**(B). This close similarity is captured by the calculations for C5/C6a($a$) and C5/C6a($g_-$), two structures that differ in the position of the aromatic ring. Given their large energy difference, it seems likely that C5/C6a($a$) is B, while C5/C6a($g_-$) is E. The TDDFT calculations are consistent with this choice, with the $S_0-S_1$ separation in the *anti* position well below that for ($g_-$) (Table S4, Supporting Information).

The middle panel of Figure 10 compares the experimental spectrum of **αβL**(D) with several best-fit structures, all of which belong to the C7/C8 family. The spectrum is closely similar to that of **βαL**(D) in the amide NH stretch region (Figure 8). This is not unexpected, since many of the α/β-peptide conformers (**αβL**) should have a partner with similar H-bonding patterns in the βα analogue **βαL**. In this case, the position of the $S_0-S_1$ origin is quite different, reflecting differences in the way the aromatic ring interacts with the C7/C8 and C8/C7 peptide backbones in the two cases.

The remaining conformers of **αβL**, C and F, have unusual NH stretch spectral signatures unlike those seen in either **βαL** or **βαD**. Conformer C has a single strong H-bond with NH stretch shifted down to 3274 $cm^{-1}$, lower than in any other conformer so far discussed. In **βαL** and **βαD**, the only types of structures that could produce NH stretch fundamentals with shifts near to this were C8/C7 double-rings, with the C8 ring responsible for the NH stretch with the largest shift. In **αβL**, however, vibrational frequency calculations predict the strongest

***Table 2.*** Experimentally Observed and Preferred Conformational Families of Model α-, β-, and α/β-Peptide Molecules

| peptide type | molecule | observed families | preferred families |
|---|---|---|---|
| α-peptides | Ac-Ala-NHMe[a] | C5, $C7_{eq}$ | $C7_{eq}$ |
| | Ac-Phe-NHMe[b] | C5, $C7_{eq}$ | C5[d] |
| | Ac-L-Ala-L-Phe-$NH_2$[c] | $C7_{eq}/C7_{eq}$, C10 (type I) | $C7_{eq}C7_{eq}$ |
| | Ac-D-Ala-L-Phe-$NH_2$[c] | C10 (type II′) | C10 (type II′) |
| | Ac-L-Phe-L-Ala-$NH_2$[c] | $C5/C7_{eq}$ | $C5/C7_{eq}$[d] |
| | Ac-L-Phe-D-Ala-$NH_2$[c] | $C5/C7_{eq}$ | $C5/C7_{eq}$[d] |
| β-peptides | Ac-$\beta^3$-hPhe-NHMe[e] | C6, C8 | C6 |
| | Ac-$\beta^3$-hAla-$\beta^3$-hPhe-NHMe[f] | C6/C6,C10,C8/C8,(C6/C8) | C6/C6 and C10 |
| | Ac-$\beta^3$-hPhe-$\beta^3$-hAla-NHME[f] | C6/C6/ C10, C8/C8, (C6/C8) | C6/C6 and C10 |
| α/β-peptides | Ac-$\beta^3$-hAla-L-Phe-NHMe (**βαL**) | *g* | $C8/C7_{eq}$ and C6/C5 |
| | Ac-$\beta^3$-hAla-D-Phe-NHMe (**βαD**) | *g* | $C8/C7_{eq}$ and C11 |
| | Ac-L-Phe-$\beta^3$-hAla-NHMe (**αβL**) | *g* | C5/C8 and C5/C6 |

[a] Reference 73 [b] Reference 13 [c] References 10−12, 25, 27 [d] Phe side chain forms NH···π H-bond with NH not involved in C5 ring. [e] Reference 8 [f] Reference 9 [g] See Table 1 for details.

hydrogen bonded NH corresponds to NH(2) when forming a C7 hydrogen bonded ring, therefore, we surmise that the red shift observed is due to the presence of a C7 ring. The other two NH stretch fundamentals (3436 and 3440 $cm^{-1}$) are in a region lower than expected for free amide NH groups, but above most weak H-bonds. The bifurcated double-ring structure $C7_{eq}$/C11($g_-$) shows the correct overall pattern, and as such may suffer from the same deficiencies as other bifurcated double-ring structures in not reproducing the experimental shifts accurately. Finally, **αβL**(F) has an NH stretch spectral pattern reminiscent of **βαL**(E), with three closely spaced fundamentals (3440, 3444, and 3467 $cm^{-1}$) with little or no H-bonding present. An extensive search for possible structures uncovered the possibilities shown in the right panel of Figure 10. The anticipated presence of C11 conformers and the presence of low-energy C5 conformers in **αβL** leads the lack of a firm assignment based on the present data.

## 4. Discussion

The present study has detected and spectroscopically characterized a total of 18 conformational isomers, six for each of the molecules **βαL**, **βαD**, and **αβL**. Throughout our discussion, the α-peptide and β-peptide analogues form natural points of comparison that can shed light on the α/β-peptide preferences. Table 2 summarizes the observed and preferred conformations found in previous studies on α- and β-peptides.[8−13,25,27,73] In the absence of an aromatic side chain, the diamide Ac-Ala-NHMe prefers the $C7_{eq}$ conformation,[73,74] while in its presence (Ac-Phe-NHMe), the C5 ring is preferred,[13] since this conformation enables the second NH to form an NH···π H-bond with the aromatic ring. In the α-peptide triamide Ac-Phe-Ala-$NH_2$, the local preferences of Phe and Ala side chains are favored in forming $C5/C7_{eq}$ structures.[10,11] Interestingly, these structures contain HXH three-center or bifurcated H-bonds,[10,75,76] in which the central C=O group (C=O(2)) accepts two H-bonds, from NH(1) in forming the C5 ring and NH(3) to form a C7 ring. Such bifurcated H-bonds have been shown in previous studies on α-peptides to be energetically stabilized relative to a single H-bond, but there is an anticooperative effect, with each component O--H interaction in the HXH system lengthened and weakened relative to such an O--H interaction in isolation.[75,76] In the $C5/C7_{eq}$ case, the C5 H-bond is so weak that this anticooperativity is small. Nevertheless, when the Phe and Ala side chains are reversed in Ac-L-Ala-L-Phe-$NH_2$, $C7_{eq}/C7_{eq}$ double-ring structures dominate, in which the central amide NH forms one H-bond while its C=O group accepts another. A minor C10 single-ring conformer is also observed.[11,12] In the D-Ala-L-Phe diastereomer,[27] a C10 ring is the only structure observed. Thus, the α-peptide analogues show a delicate balance between $C5/C7_{eq}$, $C7_{eq}/C7_{eq}$ and C10 structures.

In the β-peptide Ac-$\beta^3$-hPhe-NHMe, both C6 and C8 conformers are observed, but transitions due to the C6 conformer are more than ten times as intense as those due to C8.[8] This preference for C6 over C8 rings carries through to the double-ring structures in Ac-$\beta^3$-hPhe-$\beta^3$-hAla-NHMe and Ac-$\beta^3$-hAla-$\beta^3$-hPhe-NHMe, where C6/C6 structures are among the major conformers, while C8/C8 structures are present at most as minor conformers.[9] Both these molecules also have the larger C10 single-rings as major conformers, independent of the order of Phe and Ala side chains. C8/C6 or C8/C12 bifurcated double-ring structures were tentatively assigned as minor conformers, with unusual NH stretch IR spectra consistent with more significant anticooperativity between the component O--H interactions.

**4.1. Conformational Preferences of α/β-Peptides.** In the α/β-peptides studied here, **βαL**(Ac-$\beta^3$-hAla-α-Phe-NHMe) and **αβL**(Ac-α-Phe-$\beta^3$-hAla-NHMe) are prototypical α/β-peptides differing in the order of α- and β-peptide subunits. **βαL** and **βαD** differ in chirality at the C(α) carbon of the α-peptide subunit. The comparison yields several general conclusions. First, in the set of three molecules, representative examples of several conformational families are found, including single ring (C11), sequential double ring (C8/C7, C7/C8, C6/C5, C5/C6), and bifurcated double-ring (C5/C8 and possibly C7/C11). This diversity of conformational families is in keeping with the small energy differences predicted by calculations among the lowest-energy structures of each type (Figure 7), a result not surprising in light of the close energetic proximity among competing structures in the α- or β-peptide analogues.

Second, while sequential double-ring structures are preferred in **βαL** and **αβL**, C11 single-rings are nearby in energy, with the **βαD** diastereomer having one of its two major conformers a C11 structure, analogous to the C10 conformers observed in the β-peptide analogues. It is interesting that the larger single-rings compete under any conditions, since they have one less H-bond, and thereby cannot experience cooperative strengthen-

(73) Lavrich, R. J.; Plusquellic, D. F.; Suenram, R. D.; Fraser, G. T.; Walker, A. R. H.; Tubergen, M. J. *J. Chem. Phys.* **2003**, *118*, 1253.
(74) Improta, R.; Barone, V. *J. Comput. Chem.* **2004**, *25*, 1333.
(75) Yang, J. H.; Christianson, L. A.; Gellman, S. H. *Org. Lett.* **1999**, *1*, 11.
(76) Yang, J. H.; Gellman, S. H. *J. Am. Chem. Soc.* **1998**, *120*, 9090.

ing. The large single-rings do afford more extensive dispersive attractions within the ring, which must counter-act their weaker H-bonding.

Third, in ***β*αL**, the two major sequential double-rings (C8/$C7_{eq}$ and C6/C5) bring together the stronger α-peptide ring ($C7_{eq}$) with the weaker β-peptide ring (C8), and vice versa. This is because C6/$C7_{eq}$ double-rings involving the two stronger single rings produce a bifurcated double-ring (Figure 6, lower left) with its attendant destabilization.

Fourth, ***β*αL** and **α*β*L** prefer different double-ring structures. In ***β*αL**, C8/$C7_{eq}$ conformers dominate (A, C, D), with a single C6/C5 conformer (G) with significant intensity. In contrast, the two dominant conformers of **α*β*L** are C5/C8 (A) and C5/C6 (B), with a single C7/C8 conformer present only as a minor conformer (D). The switch in conformational preferences from C8/$C7_{eq}$ in ***β*αL** to C5/C8 and C5/C6 in **α*β*L** is the same switch observed by Mons and co-workers for the α-peptide analogues (Table 2),[11] with the Phe substituent dictating $C7_{eq}$ structures in the C-terminal position, but C5 in the N-terminal position. It would appear that in this pair of α/β-peptides, the preferences of the α-peptide unit dictate the overall preferences observed.

While the C5 ring is clearly preferred in **α*β*L**, it pairs with both C6 and C8 β-peptide rings with equal facility. C7/C6 structures are particularly disfavored because they are bifurcated or three-center XHY H-bonds in which a single NH group (NH(2)) forms H-bonds simultaneously with two C=O groups.[76] The large-population C5/C8 structure (**α*β*L**(A)) is particularly intriguing, because C5/C8 structures are bifurcated double-ring structures that are a composite of two less stable single-ring structures. In many cases, the counter-balancing effect is the additional stabilization arising from the interaction of the free amide NH(a+1) with the Phe side chain when it is in *anti* ring position (a) (Figure 5). The other dominant conformer of **α*β*L** is **α*β*L**(B), assigned to a C5/C6 structure. Its C6/C5 analogue in ***β*αL** is also present with large intensity (***β*αL**(G)). Both structures pair the C5 ring with the more stable C6 ring. These structures mirror the C6/C6 double rings that are most stable in the β-peptide analogues. Thus, while the α-peptide unit plays a significant role in dictating the overall conformational preference, the β-peptide subunit also plays a role. In these structures, the high frequency of the free amide NH stretch (3500 $cm^{-1}$) argues against stabilization by an NH···π H-bond, pointing instead to the inherent stability of the C6 ring as primarily responsible for the stability of the C5/C6 double rings.

**4.2. Diastereomer-Specific Effects.** Availability of the homochiral and heterochiral diastereomers ***β*αL** and ***β*αD** has provided the opportunity to explore in some detail the effects of changes in one chiral center on the ultraviolet and infrared spectra of Ac-$\beta^3$-hAla-Phe-NHMe. R2PI, UVHB, and RIDIR spectroscopies confirmed that six unique conformers were present in the supersonic expansion for both ***β*αL** and ***β*αD**.

While the overall spectral signatures of each diastereomer are quite different (Figures 13), certain conformers of ***β*αL** and ***β*αD** form diastereomeric pairs in which the chirality change has made little difference. Three such diastereomeric pairs have been noted and labeled as such: A/A′, C/C′, and G/G′. The $S_0-S_1$ origin transitions of the two members of each pair appear within a few $cm^{-1}$ of one another (Table 1), indicating that the phenyl ring interacts with its local surroundings in near-identical fashion. Changes in chirality at the α-peptide subunit effectively swaps the (*a*) and ($g_-$) phenyl ring positions, but leaves the $g_+$ position unchanged. Since the IR spectral differences are also small, we are assured that the pair belongs to the same peptide backbone family. Thus, we anticipate that the two members of each diastereomeric pair will form a Cn/Cm(*a*)↔Cn/Cm($g_-$) pair or both be assigned as Cn/Cm($g_+$).

These additional constraints lead to a refinement in the assignments for these diastereomeric pairs beyond the set of possible structures shown in ***β*αL**(A)/***β*αD**(A′) pair, we see that assignment of ***β*αL**(A) to C8c/$C7_{eq}$(*a*) and ***β*αD**(A′) to C8d/$C7_{eq}$($g_-$) is consistent with their near-identical $S_0-S_1$ origins, but allows for small differences in NH stretch spectra associated with changes in dihedral angles in the C8c versus C8d rings. Furthermore, these structures both have the C=O(3) group interacting with the aromatic ring, a local environment consistent with the observed position of the $S_0-S_1$ origin on the blue edge of the observed conformers, as predicted by TDDFT calculations (Tables S3 and S4, Supporting Information). Similar reasoning leads to assignment of the ***β*αL**(C)/***β*αD**(C′) pair as C8a/$C7_{eq}$(*a*)↔C8a/$C7_{eq}$($g_-$). Finally, the ***β*αL**(G)/***β*αD**(G′) diastereomeric pair can be assigned as C6b/C5(*a*) ↔C6b/C5($g_-$). In this case, the aromatic ring position facilitates an NH(3)···π interaction, which is evidenced by the red shift of the free amide NH transition in the IR spectra and in the red shift of the $S_0-S_1$ origin transitions of these C6/C5 conformers.

The presence of three chiral pairs with near-identical spectral properties is an intriguing, but somewhat anticipated result of the change in a single chiral center. More interesting is the fact that the remaining conformers of ***β*αL** and ***β*αD** do not have clear diastereomeric counterparts. In fact, ***β*αD**(B) has the most intense transition in the R2PI spectrum (Figure 3), but its only plausible C11 counterpart in ***β*αL** is ***β*αL**(F), the smallest of the six conformers of ***β*αL**, with only a tentative assignment to C11. By contrast, in ***β*αL**, conformer G is a major conformer assigned to a C6/C5 structure, while in ***β*αD**, G′ is the least intense of the six conformers in the R2PI spectrum. Thus, while both ***β*αL** and ***β*αD** spread significant population over several C8/C7 double-ring structures, there is an apparent trade-off in the relative intensities of C6/C5 and C11 conformers, with ***β*αL** favoring C6/C5 over C11, while ***β*αD** favors the reverse.

In this case, the lack of a diastereomeric counterpart appears to be due to a real energetic difference associated with the change in chirality in the α-peptide subunit. The ***β*αL** and ***β*αD** energy level diagrams in Figure 7 show trends in relative energies that track, at least generally, the shifts in population observed. In ***β*αD**, the C11 structure is the calculated global minimum, in keeping with the observation of ***β*αD**(B) as a large population conformer. By comparison, the lowest-energy C6/C5 structure is over 6 kJ/mol higher in energy at the DFT M05-2X/6-31+G(d) level of theory. In ***β*αL**, on the other hand, the lowest-energy C6/C5 and C11 structures are less than 3 kJ/mol apart, consistent with the observed shift in population from C11 toward C6/C5.

In seeking an explanation for the stability of the C11(g+) conformation of ***β*αD** over the C11($g_+$) conformation of the diastereomer ***β*αL**, we carried out calculations to see whether these stability difference were evident in the α-peptide subunit itself that contained the changed chiral center. Figure 11a) shows optimized structures of the C11($g_+$) diastereomers of ***β*αL** and ***β*αD**. The shaded regions show the effect of the chirality change on the orientation of the amide NH group relative to the $\beta^3$ CH: these bonds are eclipsed in ***β*αL** but *anti* in ***β*αD**. To determine whether this local structural change was the source of a stability difference, calculations were carried out on the corresponding conformers of *N*-isopropylacetamide, formed from the structures in Figure 11a) by cutting the two structures

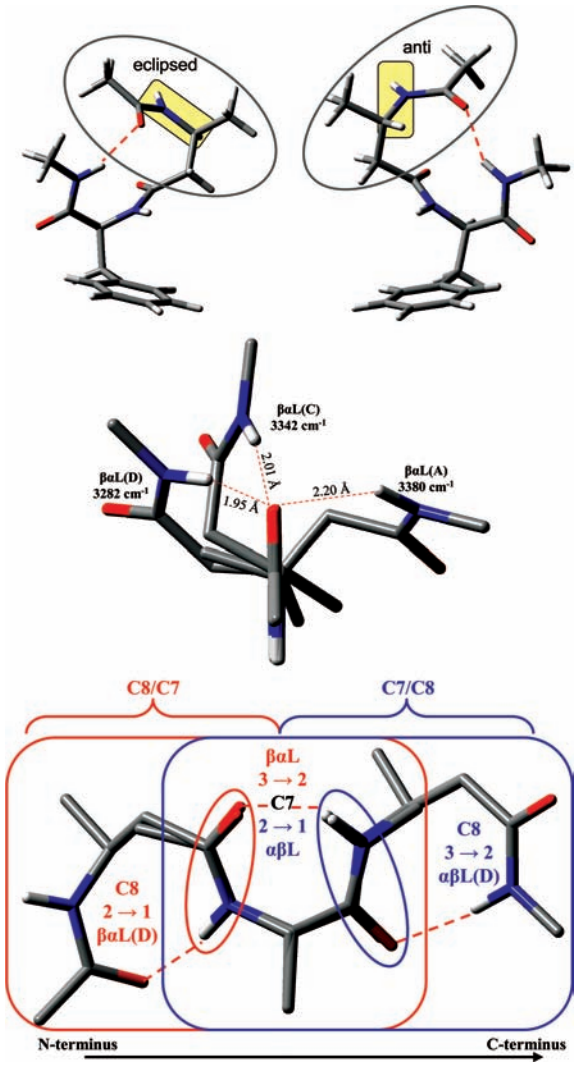


***Figure 11.*** (a) C11($g$+) structures for ***β*αL** and ***β*αD**. (b) Overlay of the C8 H-bonded rings of conformers A, C, and D of ***β*αL**. Included are RNH···O distances from the B3LYP/6-31+G(d) optimized geometries. Alkyl hydrogen atoms and the α-residue are removed for clarity. (c) Overlay of the peptide backbones (aligned via their $C7_{eq}$ rings) of the $C8/C7_{eq}$ structure assigned to ***β*αL**(D) (red rectangle) and the $C7_{eq}$/C8 structure (blue rectangle) assigned to ***αβ*L**(D). The central amide group that acts as both a donor and acceptor is highlighted in red (***β*αL**(D)) and blue (***αβ*L**(D)).

at the C($\beta^2$)−C(=O) bond and replacing it with a C($\beta^2$)-H. After optimization, the two structures differ by 8−10 kJ/mol, with structure formed from ***β*αD** lower in energy than the structure formed from ***β*αL**. The optimized structures point to steric effects between the $\beta^2$ methylene group and the C=O group as the source of this stability difference, with the structure arising from ***β*αD** C11(g+) minimizing these repulsions. We surmise on this basis that the difference in stability of the two diastereomeric C11(g+) structures arises from this same effect, leading to the observed shift in population toward C11(g+) in ***β*αD** compared to ***β*αL**.

More generally, the shift toward large single-ring in the heterochiral diastereomer ***β*αD** is the same one observed in the α-peptide analogues (Table 2), in that case from $C7_{eq}/C7_{eq}$ double-ring to C10 single-ring. In the α-peptides, the effect is more dramatic, with only $C7_{eq}/C7_{eq}$ observed in one, and only C10 in the other. In order to better compare and contrast the diastereomeric shifts in population and their dependence on peptide type (α-, $\beta$-, or α/$\beta$-), further experimental and theoretical exploration of the potential energy surfaces is required, particularly regarding the energy barriers separating conformational families.

**4.3. The C=O Group as H-Bond Acceptor.** One striking aspect of the single-conformation infrared spectra of these model α/$\beta$-peptides is the large variation in the NH stretch frequencies within the set of seven $C8/C7_{eq}$ structures formed by ***β*αL** and ***β*αD**. One might expect a natural trade-off in such double-rings, with formation of a strong C8 H-bond occurring at the expense of the strength of the C7 H-bond, and vice versa. However, if one uses the wavenumber positions of the NH stretch fundamentals as a reflection of the strengths of these H-bonds, there is little obvious correlation; that is, one cannot generally associate a shift down in frequency in the C8 NH stretch with a shift up in the C7 NH stretch. Instead, while the C7 NH stretch fundamentals are typically within about 20 $cm^{-1}$ of one another, the C8 fundamentals vary by almost 100 $cm^{-1}$ from one structure to the next.

Table 3 correlates the observed and calculated amide NH stretch frequencies for the C8 and $C7_{eq}$ H-bonds with the calculated structural parameters for these H-bonds based on their assigned structures. Figure 11b) presents a pictorial view of the C8 H-bonds formed in conformers A, C, and D of ***β*αL**, whose NH stretch fundamentals appear at 3380, 3342, and 3282 $cm^{-1}$, respectively. As one can immediately see, the three NH groups forming C8 H-bonds approach the C=O group from very different distances and approach angles. The primary correlation between NH stretch frequency and structure is with the distance between the donating H and accepting O ($R_{NH...O}$). The shorter the distance, the lower the frequency of the NH stretch fundamental, as is typically assumed in correlating a larger NH shift with a stronger H-bond. However, while one might anticipate a preference for NH approach angles that point the NH bond toward the oxygen lone pairs, in or near the amide acceptor plane (as in ***β*αL**(C)), the NH group in ***β*αL**(D) is nearly perpendicular to the acceptor amide plane, yet it produces the lowest frequency NH stretch fundamental. The conformer with the highest frequency NH stretch (***β*αL**(A)) has the donor amide NH approaching from a highly skewed angle in which the N−H and C=O groups point nominally in the same direction.

In summary, the data set presented in this work illustrates the exceptional ability of the C=O group to accept H-bonds over a very wide range of approach geometries, making it an unusually versatile H-bond acceptor. In this sense, it is perhaps best to think of the carbonyl group as a cylinder of electron density in which the two lone pairs and $\pi$ electrons all can play a role in accepting H-bonds. This versatility is put to extraordinarily good use in the variety of secondary structures present in both synthetic foldamers and proteins.[77−81]

**4.4. Cooperative effects in sequential double-ring structures.** The triamide molecules considered here are the smallest heterogeneous polypeptides that have both terminal and interior amide groups. As such, they can provide insight to the effects of multiple H-bonds involving the same amide group. In larger polypeptides, cooperative effects play an important

(77) Mitchell, J. B. O.; Price, S. L. *Chem. Phys. Lett.* **1989**, *154*, 267.
(78) Taylor, R.; Kennard, O.; Versichel, W. *J. Am. Chem. Soc.* **1983**, *105*, 5761.
(79) Taylor, R.; Kennard, O.; Versichel, W. *Acta Crystallogr., Sect. B* **1984**, *40*, 280.
(80) Taylor, R.; Kennard, O.; Versichel, W. *J. Am. Chem. Soc.* **1984**, *106*, 244.
(81) Baker, E. N.; Hubbard, R. E. *Prog. Biophys. Mol. Biol.* **1984**, *44*, 97.

***Table 3.*** Calculated Structural Parameters from the B3LYP/6-31+G(d) Optimized Geometries for the C8/$C7_{eq}$ Conformers of **βαL** and **βαD** and the $C7_{eq}$/C8 Conformer of **αβL**; also Included for Comparison Are the Experimental Amide NH Stretch Frequencies for the C8 and $C7_{eq}$ H-Bonded Rings

| | | C8 | | | | | | | C7 | | | | | | |
|---|---|---|---|---|---|---|---|---|---|---|---|---|---|---|---|
| conformer | assignment | $R_{NH\cdots O}$ (Å)[a] | $R_{N-O}$ (Å)[a] | $R_{N-H}$ (Å)[a] | NHO angle (deg)[a] | COH angle (deg)[a] | calc. freq. ($cm^{-1}$)[b] | expt. freq. ($cm^{-1}$) | $R_{NH\cdots O}$ (Å)[a] | $R_{N-O}$ (Å)[a] | $R_{N-H}$ (Å)[a] | NHO angle (deg)[a] | COH angle (deg)[a] | calc. freq. ($cm^{-1}$)[b] | expt. freq. ($cm^{-1}$) |
| **βαL**(A) | C8c/$C7_{eq}(a)$ | 2.200 | 3.045 | 1.017 | 139 | 98 | 3387 | 3380 | 2.188 | 2.987 | 1.016 | 134 | 110 | 3396 | 3389 |
| **βαL**(C) | C8a/$C7_{eq}(g_-)$ | 2.018 | 2.999 | 1.021 | 160 | 131 | 3332 | 3342 | 2.036 | 2.932 | 1.018 | 145 | 104 | 3361 | 3398 |
| **βαL**(D) | C8b′/$C7_{eq}(g_-)$ | 1.957 | 2.957 | 1.022 | 165 | 105 | 3298 | 3282 | 2.059 | 2.940 | 1.017 | 143 | 104 | 3374 | 3374 |
| **βαD**(A′) | C8d/$C7_{eq}(g_-)$ | 2.239 | 3.088 | 1.017 | 140 | 95 | 3393 | 3385 | 2.233 | 3.012 | 1.016 | 132 | 110 | 3405 | 3373 |
| **βαD**(C′) | C8a/$C7_{eq}(a)$ | 2.035 | 3.014 | 1.021 | 160 | 131 | 3331 | 3331 | 2.050 | 2.950 | 1.018 | 146 | 103 | 3365 | 3357 |
| **βαD**(X) | C8b/$C7_{eq}(a)$ | 1.967 | 2.956 | 1.020 | 162 | 99 | 3321 | 3321 | 2.017 | 2.906 | 1.018 | 144 | 107 | 3355 | 3365 |
| **βαD**(Y) | C8b/$C7_{eq}(g_-)$ | 1.955 | 2.947 | 1.021 | 163 | 99 | 3306 | 3293 | 2.107 | 2.951 | 1.017 | 139 | 108 | 3384 | 3390 |
| **αβL**(D) | C8b/$C7_{eq}(g_-)$ | 1.984 | 2.968 | 1.017 | 161 | 102 | 3367 | 3399 | 1.969 | 2.903 | 1.022 | 150 | 101 | 3301 | 3314 |

[a] B3LYP/6-31+G(d). [b] B3LYP/6-31+G(d) frequencies scaled by 0.96.

role in stabilizing larger secondary structures (e.g., helices or beta sheets).[82−86] However, the present single-conformation spectroscopy results provide an especially clear view of their spectroscopic consequences.

In all the sequential double-ring structures (Figure 5) the central amide group (2) acts as both donor and acceptor in H-bonds with adjacent amide groups (a→a ± 1). In the C8/$C7_{eq}$ double-ring structures of **βαL** and **βαD**, the NH(2)→C=O(1) H-bond forms a C8 ring, while in **αβL** the swapping of α and β-peptide subunits produces a $C7_{eq}$ ring for this same 2→1 H-bond. This is illustrated in Figure 11c), where the $C7_{eq}$ rings of **βαL**(D) and **αβL**(D) are overlaid. These two structures were chosen because their H-bond structural parameters are similar to one another (Table 3).

As the stick diagrams in Figures 8−10 show, in all three molecules, the lowest frequency NH stretch in the C8/C7 and C7/C8 double-ring structures is always the central amide NH(2). This NH group acts as donor in a C8 ring in **βαL** and **βαD**, but forms a C7 ring in **αβL**. We surmise, then, that in both C8/C7 and C7/C8 double-rings, it is the central amide NH stretch that is lowest in frequency, independent of the order of the C8 and C7 rings.

The comparison between **βαL**(D) and **αβL**(D) (Figure 11c) and Table 3) provides a quantitative measure of these effects. Most of the structural parameters of the C8 and $C7_{eq}$ H-bonds in this pair are quite similar; yet, the cooperatively strengthened C8 NH stretch in **βαL**(D) is 117 $cm^{-1}$ lower in frequency than its counterpart in **αβL**(D), which cannot experience cooperative effects. Similarly, the central $C7_{eq}$ NH stretch fundamental of **αβL**(D) is at 3314 $cm^{-1}$, 60 $cm^{-1}$ lower in frequency than its counterpart in **βαL**(D). One might have thought that this frequency shift would result from a shortening of the NH···O=C H-bond involving the central amide NH; however, most of the structural parameters in **βαL**(D)/**αβL**(D) pair are not changed significantly, particularly in the C8 ring.

The single structural parameter most directly related to the observed frequency changes is the NH bond length of the central amide, which increases in length by ∼0.005 Å when it is both donor and acceptor, where cooperative effects can occur. In **βαL**(D) it is the NH bond in the C8 ring that lengthens, while in **αβL**(D) it is the NH in the $C7_{eq}$ ring. This is the same structural effect that accompanies shortening the $R_{NH\cdots O}$ H-bond distance in the **βαL**(A→C→D) series. Thus, the shift in NH stretch frequency that we ascribe to a cooperative effect has an electronic origin, which leads to a lengthening of an amide N−H bond in response to the C=O of that amide serving as an H-bond acceptor. This bond lengthening is consistent with the notion that H-bonding interactions involve transfer of electron density from the acceptor (the carbonyl oxygen in this case) to the N−H antibonding orbital.[87−90] However, here it is the carbonyl oxygen on the *same* amide group that produces the effect through the amide bond to the NH when this carbonyl oxygen accepts a H-bond from another NH group.

Similar reasoning carries over to the C6/C5 and C5/C6 rings, where the effects are less dramatic. As the labels on the stick spectra of Figure 10 indicate, in **αβL**(B) and **αβL**(E), the central amide group acts as H-bond donor in a C6 ring (2→3) and acceptor in a C5 ring (1→2). The C6 amide NH stretch is lowest in frequency, as we would have anticipated based on the relative strengths of the C6 and C5 single rings, with a separation between C6 and C5 NH stretch fundamentals of about 45 $cm^{-1}$. In the C6/C5 analogues **βαL**(G) and **βαD**(G′), the central amide NH(2) forms a C5 ring, with its carbonyl group (C=O(2)) acting as acceptor in a C6 ring. This double interaction pushes the C5 NH stretch fundamental down to ∼3420 $cm^{-1}$, over 50 $cm^{-1}$ below its free value (Table 1), and reduces the separation between C6 and C5 NH stretch fundamentals to only 15 $cm^{-1}$. Thus, cooperative effects in the C5 ring does not swap the order of the C5 and C6 fundamentals, but does reduce their frequency separation quite substantially, lowering the C5 NH stretch fundamental to values within about 20 $cm^{-1}$ of typical frequencies found for C6 (∼3400 $cm^{-1}$) and $C7_{eq}$ (∼3400 $cm^{-1}$) single rings.[8,11]

Since the relative energies of conformers depend on a delicate balance of attractions and repulsions within a molecule, it is difficult to make a quantitative assessment of the increase in H-bond strength that arises from cooperative effects reflected in a given NH stretch frequency shift. Future conformation-specific studies of this type on larger polypeptides can probe this relationship more fully as the network of H-bonds evolves in size.

(82) Guo, H.; Karplus, M. *J. Phys. Chem.* **1992**, *96*, 7273.
(83) Koch, O.; Bocola, M.; Klebe, G. *Proteins* **2005**, *61*, 310.
(84) Ludwig, R.; Reis, O.; Winter, R.; Weinhold, F.; Farrar, T. C. *J. Phys. Chem. B* **1998**, *102*, 9312.
(85) Ludwig, R.; Weinhold, F.; Farrar, T. C. *J. Chem. Phys.* **1995**, *103*, 3636.
(86) Sheridan, R. P.; Lee, R. H.; Peters, N.; Allen, L. C. *Biopolymers* **1979**, *18*, 2451.
(87) Reed, A. E.; Curtiss, L. A.; Weinhold, F. *Chem. Rev.* **1988**, *88*, 899.
(88) Reed, A. E.; Weinhold, F. *J. Chem. Phys.* **1983**, *78*, 4066.
(89) Weinhold, F. Resonance character of hydrogen-bonding interactions in water and other H-bonded species. In *Peptide Solvation and H-Bonds: Advances in Protein Chemistry*; Baldwin, R. L., Baker, D., Eds.; Elsevier, 2006; Vol. 72; p 121.
(90) Weinhold, F.; Landis, C. R. *Valency and Bonding*; Cambridge University Press; New York, 2005; Sec. 5.2.

## 5. Conclusions

In this study, conformation- and diastereomer-specific spectroscopy has been used to record the UV and IR spectra of three model peptides, Ac-$\beta^3$-hAla-L-Phe-NHMe (***βα*L**), Ac-$\beta^3$-hAla-D-Phe-NHMe (***βα*D**), and Ac-L-Phe-$\beta^3$-hAla-NHMe (**α*β*L**), isolated and cooled in a supersonic expansion. The conformational preferences of these molecules depend sensitively on the order of the α- and $\beta$-amino acid residues (***βα*L** vs ***βα*L**) and the configuration of the phenylalanine residue (***βα*L** vs ***βα*D**). In ***βα*L** and ***βα*D**, C8/C7 double-ring structures dominate, while a single C6/C5 conformer in ***βα*L** is reduced in population relative to a C11 counterpart present in ***βα*D**. When the α-peptide subunit is in the N-terminal position, as it is in **α*β*L**, this subunit prefers to form the C5 ring, much as it does in α-peptides.[11,13] Both C5/C8 and C5/C6 conformers dominate the spectrum. The spectra reveal a total of 18 conformational isomers for the three molecules, oftentimes with at least one member represented from several conformational families. This observed conformational diversity is in keeping with potential energy surfaces that divide into conformational family subspaces with relatively high barriers between them, thereby trapping the high-temperature equilibrium population and collecting it into one or a few of the lowest-energy structures of a given type.[11] This data set thus provides the spectral signatures of C8/C7, C11, C6/C5, C5/C8, C5/C6, and C7/C8 families. Future studies will involve examination of constrained α/$\beta$-peptides in which the $\beta$-peptide subunit is part of a cyclopentane ring (ACPC).

**Acknowledgment.** W.H.J., E.E.B., V.A.S., and T.S.Z. acknowledge support for this research from the National Science Foundation (NSF-CHE0551075). S.H.G. and S.H.C. were supported by NSF Grant CHE-0551920; in addition, S.H.C. was supported in part by a fellowship from the Samsung Scholarship Foundation.

**Supporting Information Available:** Synthetic procedures; structures of C6, C7, C8 ring types; structural parameters, relative energies, and $S_0-S_1$ energy separations for ***βα*L**, ***βα*D**, and **α*β*L**; complete version of reference 40 This material is available free of charge via the Internet at http://pubs.acs.org.

JA901051V